

Charles University in Prague
Faculty of Science

DIPLOMA THESIS



Zdeněk Preisler

Computer Modeling of Branched Polymers

Department of Physical and Macromolecular Chemistry

Thesis Supervisor: RNDr. Filip Uhlík, Ph.D.

Study Program: Chemistry

Branch of Study: Physical Chemistry

2010

I would like to thank to all, without whom this work would not be possible, at first place to my supervisor RNDr. Filip Uhlík Ph.D. for a great help and support, then to Frans Leemakers from University of Wageningen, the Netherlands, for his help and discussions, without him the SCF calculation would not be possible. Also to our professor Karel Procházka, without whom nothing of this would be possible. It was a great pleasure to be part of his group. I would also like to thank to Doc. Ing. Zuzana Limpouchová CSc. and to Mgr. Peter Košovan Ph.D.

I would like to acknowledge the Grant Agency of the Academy of Sciences of the Czech Republic, grant GAAV IAA400500703 and the Ministry of Education, Youth and Sports of Czech Republic, grant MSMT MSM0021620857.

thank you

I, hereby, declare I have written my diploma thesis by myself and all used literature has been cited. I agree that this work may be lent and published.

– Zdeněk Preisler (2010)

Abstract

In this work we study properties of branched polymers in a good solvent. We focus on problematic related to the size exclusion chromatography and predicting elution behavior of randomly branched polymers. We developed a software for generating self-avoiding walks (SAW) of any given non-looping architecture on a cubic lattice using Monte Carlo (MC) simulation and validate its reliability by presenting the scaling of different architectures: linear, 3-arm star and 6-arm star and asymmetric star. We calculate distribution coefficients and calibration curves for size exclusion chromatography for various architectures to validate that the hydrodynamic radius is more suitable for predicting elution volume than the radius of gyration. Then we propose a new method for, although approximate, a very fast estimation of radius of gyration and hydrodynamic radius for different architecture using a graph method. It is done by comparing MC results with results obtained from graph theory. Then we introduce a correction to graph-theory results to fit the MC. At the end we present depletion layer calculation from MC and self-consistent field (SCF) method for polymers and their comparison. We show how calculation of depletion layer using SCF can be improved to get significantly better agreement with MC results.

Contents

Contents	vii
Introduction	ix
1 Properties of Polymer Chains	1
1.1 Ideal Polymer Chain	1
1.1.1 Freely Jointed Chain Model	2
1.1.2 Gaussian Chain	3
1.2 Radius of Gyration	4
1.3 Real Polymer Chains	5
1.3.1 Excluded Volume Chain Models	5
1.3.2 Flory-Huggins Theory	7
1.3.3 Regimes of Polymer Solutions	8
1.3.4 Flory Exponent	9
1.4 Fluctuation Theory and Scaling Concepts	10
1.4.1 Scaling	10
1.4.2 Perturbation Theory	11
1.4.3 Renormalization Group Theory	12
1.5 Dynamical Properties	12
1.5.1 Rouse Model	12
1.5.2 Zimm model	13
1.5.3 Hydrodynamic Radius	15
2 Monte Carlo	17
2.1 Monte Carlo Integration	17
2.2 The Metropolis Method	18
2.3 The Rosenbluth & Rosenbluth Method	22
3 Monte Carlo Calculations	25
3.1 Algorithm Implementation	25
3.1.1 Remark on Bracket Notation	26
3.2 Calculation of Averages	27
3.2.1 Autocorrelation Function	27

3.2.2	Block Method	28
3.3	Scaling	29
3.4	Distribution Coefficient Calculations	31
3.5	Depletion Layer Calculation	35
3.6	Graph Theory Calibration	36
3.6.1	Graph Theory	36
3.6.2	Coarse Graining	37
3.6.3	Comparison of MC and Graph Theory	38
3.6.4	Hydrodynamic Radius Calibration	39
4	Self-Consistent Field Method for Polymers	41
4.1	Introduction	41
4.2	SCF Theory	42
4.2.1	Self-Consistent Field Theory and the Molecular Model	44
4.3	The Models	47
5	Comparison of MC and SCF Results	49
5.1	Discussion	49
	References	55

Introduction

People were using naturally occurring polymers such as natural rubber or caoutchouc for centuries without realizing they are actually dealing with macromolecules. Until Staudinger in 1922 proposed a hypothesis that polymers are molecules composed of covalently bonded elementary units called monomers. Even though his hypothesis was not generally accepted by 1929, Carothers had synthesized a variety of polymers with well-defined structures.

Polymers were always of a great interest due to their various (mechanical, thermal, electrical, optical, ...) properties. We are studying these properties using molecular simulations. Molecular simulation became an established method of research in science, complementing both the analytical theory as well as the experiment. And they are still becoming more and more important as computers progress, pushing their limits to a higher and higher performance. Due to the complexity of chemical structure of polymer systems, the variability of their properties is huge. The theoretical methods often suffer from rather crude approximations, which they apply to study polymer system, and whose validity is often difficult to justify, both physically as well as mathematically. Computer simulation can often provide more complex models in a full detail without introducing serious approximations. Moreover in comparison with experiment it is possible to improve models systematically.

Despite of all the technological progress, simulating polymers is still quite challenging. Already a single chain exhibits structure ranging from size of a single chemical bond ($\approx 1 \text{ \AA}$) to the persistence length ($\approx 10 \text{ \AA}$) to the coil radius ($\approx 100 \text{ \AA}$) and the time scales from time of a chemical vibration (10^{-14} s) up to relaxation times of the whole coil (10^{-6} s). This time-scale gap is a problem, which we have to face and it is often very difficult to handle. Therefore we instead of simulating polymers of atoms simulate the behavior of an overall coarse-grained picture of polymers taking into account only segment or even larger units. This coarse-graining also brings, to some extent, elimination of fast local motions, however this approach still turns out to be very reasonable and it often brings good agreement with experiments.

In our work we focus on branched polymers in a good solvent. The branched polymers can exhibit quite different properties from their linear analogs. Branched polymers can be synthesized for example branching polyesters may be achieved by addition of glycerol. Similarly the addition of divinyl compound during chain polymerization of vinyl monomers may cause branching. You can find also natural branched polymers some of the examples are polysaccharides or lignin. There are also some special cases of branched polymers as stars, combs or dendrimer.

We are in particular interested in size exclusion chromatography, which is one of the most prevalent characterization technique for synthetic and natural polymers. There are, however, unrevealed questions and the elution behavior of branched is very difficult to predict since they can not be separated as their linear analogs, which are shown to separate proportionally to their molecular weight. This is the main topic we are trying to handle in this work.

CHAPTER 1

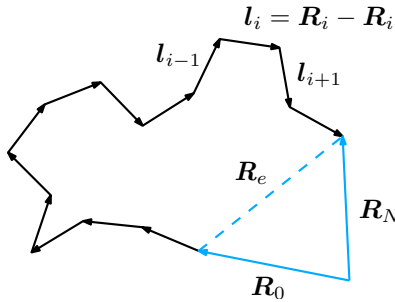
Properties of Polymer Chains

In the following text we introduce some of the very basics of polymer physics. We closely follow textbooks of Rubinstein [1], Grosberg [2], Doi [3] and de Gennes [4]. First we discuss some statical properties of ideal and real chains, scaling and in the end some of the dynamical properties of polymer chains.

1.1 Ideal Polymer Chain

The ideal chain models are important starting point in polymer physics similarly as a notion of ideal gas in traditional molecular physics. These models are represented by chain of subsequently connected links, having no interaction neither with solvent nor with other links. These models can differ in their link structure or in the type of bonding but they all neglect the excluded volume interactions.

Figure 1.1: Freely jointed chain model



1.1.1 Freely Jointed Chain Model

First, let us describe a very basic model of a polymer chain, a freely jointed chain model (see Figure 1.1) and show some of its properties. Let N be the total number of segments of length l giving $N + 1$ beads with center of mass position vectors \mathbf{R}_i , $i = 0, 1, \dots, N$. We should point out that in this model we do not account for any interactions between the segments and the bond vectors of links between subsequent beads $\mathbf{l}_i = \mathbf{R}_i - \mathbf{R}_{i-1}$ can point in any direction and the orientations of the links \mathbf{l}_i are uncorrelated. These vectors \mathbf{l}_i thus describe a random walk with a step length $l = |\mathbf{l}_i|$ through space. The total length of polymer chain with N links can be measured along the contour by sum of bond lengths

$$L = N|\mathbf{l}_i| = Nl. \quad (1.1)$$

Next, we define the end-to-end vector, \mathbf{R}_e , (Figure 1.1) to characterize the chain conformation

$$\mathbf{R}_e = \mathbf{R}_N - \mathbf{R}_0. \quad (1.2)$$

If we then calculate the mean square end-to-end vector, $\langle \mathbf{R}_e^2 \rangle$, by averaging over all conformation we can get a simple characteristics of the average coil size of the macromolecule.

Additionally we can write the end-to-end vector, \mathbf{R}_e , using the bond vectors

$$\mathbf{R}_e = \sum_{i=0}^N \mathbf{l}_i \quad (1.3)$$

and

$$\langle \mathbf{R}_e^2 \rangle = \left\langle \left(\sum_{i=0}^N \mathbf{l}_i \right)^2 \right\rangle = \sum_{i=0}^N \langle \mathbf{l}_i^2 \rangle + 2 \sum_{0 \leq i < j \leq N} \langle \mathbf{l}_i \mathbf{l}_j \rangle. \quad (1.4)$$

Since bond vectors \mathbf{l} are not correlated the angle between \mathbf{l}_i and \mathbf{l}_j ($i \neq j$) has equal probability for any value from 0 to 2π , $\langle \mathbf{l}_i \mathbf{l}_j \rangle = l^2 \langle \cos \vartheta_{ij} \rangle = 0$. $\langle \mathbf{l}_i^2 \rangle = l^2$ [2], so

$$\langle \mathbf{R}_e^2 \rangle = Nl^2 \quad (1.5)$$

meaning that the size of a polymer chain (for $N \gg 1$) $\langle \mathbf{R}_e^2 \rangle^{1/2} \sim N^{1/2}l$ is much less than its contour length Nl . Doing so we have determined the size of a coil of a freely jointed chain.

Further we introduce some flexibility of polymer. Let us consider some orientation correlation between segments so $\langle \mathbf{l}_i \mathbf{l}_j \rangle \neq 0$. Then $\langle \mathbf{l}_i \mathbf{l}_j \rangle \sim \langle \cos \vartheta_{ij} \rangle$ determines a degree of polymer flexibility. This correlation can be expressed as a mean cosine of the angle between different segments of polymer $\langle \cos \vartheta(s) \rangle$, where s is contour length between these segments.

Since this function of s has a property of multiplicity, for two neighboring sections can be rewritten as

$$\langle \cos \vartheta(s + s') \rangle = \langle \cos \vartheta(s) \rangle \langle \cos \vartheta(s') \rangle. \quad (1.6)$$

Function having this property is exponential and can be written as [2]

$$\langle \cos \vartheta(s) \rangle = \exp \left(\frac{-s}{\tilde{l}} \right), \quad (1.7)$$

where \tilde{l} is a constant for each given polymer called persistence length and it is a characteristics of polymer flexibility.

Now, let us introduce a Kuhn segment as an effective segment length. In 1934 W. Kuhn introduced another quantitative parameter of polymer chain flexibility directly associated with $\langle \mathbf{R}_e^2 \rangle$. This characteristic is now called a Kuhn segment. The length of Kuhn segment b for a long chain ($L \gg \tilde{l}$) ideal macromolecule is defined as

$$\langle \mathbf{R}_e^2 \rangle = bL. \quad (1.8)$$

Real macromolecule is then treated as a freely jointed chain of $N = L/b$ Kuhn segments. In other words Kuhn segment contains more monomer units which than taken as one behave as a segment of a freely jointed chain.

1.1.2 Gaussian Chain

Here, we mention another ideal chain model, the Gaussian chain. This model is widely used since it can be easily treated mathematically. Let us consider a chain bond length having a Gaussian distribution ψ .

$$\psi(\mathbf{l}) = \left[\frac{3}{2\pi b^2} \right]^{3/2} \exp \left(-\frac{3\mathbf{l}^2}{2b^2} \right) \quad (1.9)$$

so that

$$\langle \mathbf{l}^2 \rangle = b^2. \quad (1.10)$$

Conformational distribution function Ψ of such a chain is given by [3]

$$\Psi(\{\mathbf{l}_i\}) = \prod_{i=1}^N \left[\frac{3}{2\pi b^2} \right]^{3/2} \exp \left(-\frac{3\mathbf{l}_i^2}{2b^2} \right) \quad (1.11)$$

$$= \left[\frac{3}{2\pi b^2} \right]^{3N/2} \exp \left[-\sum_{i=1}^N \frac{3(\mathbf{R}_i - \mathbf{R}_{i-1})^2}{2b^2} \right]. \quad (1.12)$$

The Gaussian chain does not describe the local structure correctly but it correctly describe the property on large length-scales. More different ideal chain models can be described such a worm-like chain, hindered rotation model or rotational state model, etc. We will, however, not discuss them but they can be easily found elsewhere [1, 2].

1.2 Radius of Gyration

The end-to-end distance $\langle \mathbf{R}_e^2 \rangle$ is not always well defined for example for branched or ring polymers. It is convenient to use the second moment of mass distribution of polymer called radius of gyration R_g . That is average square distance between segments in a given conformation and center of mass of the polymer.

$$R_g^2 = \frac{1}{N} \sum_{i=1}^N (\mathbf{R}_i - \mathbf{R}_G)^2 \quad (1.13)$$

and

$$\mathbf{R}_G = \frac{1}{N} \sum_{i=1}^N \mathbf{R}_i \quad (1.14)$$

where \mathbf{R}_G denotes the center of mass for a particular conformation and \mathbf{R}_i denotes the vector from the first to the i -th mass point of the chain. Substituting eqn. (1.14) into eqn. (1.13) we obtain

$$R_g^2 = \frac{1}{N} \sum_{i=1}^N (\mathbf{R}_i^2 - 2\mathbf{R}_i \mathbf{R}_G + \mathbf{R}_G^2) \quad (1.15)$$

$$= \frac{1}{N} \sum_{i=1}^N \left[\mathbf{R}_i^2 - 2\mathbf{R}_i \frac{1}{N} \sum_{j=1}^N \mathbf{R}_j + \left(\frac{1}{N} \sum_{j=1}^N \mathbf{R}_j \right)^2 \right]. \quad (1.16)$$

This equation can be easily rewritten as

$$R_g^2 = \frac{1}{N^2} \sum_{i=1}^N \sum_{j=1}^N (\mathbf{R}_i^2 - 2\mathbf{R}_i \mathbf{R}_j + \mathbf{R}_i \mathbf{R}_j) \quad (1.17)$$

$$= \frac{1}{N^2} \sum_{i=1}^N \sum_{j=1}^N (\mathbf{R}_i^2 - \mathbf{R}_i \mathbf{R}_j). \quad (1.18)$$

Then this expression can be rewritten in a symmetric form

$$R_g^2 = \frac{1}{N^2} \sum_{i=1}^N \sum_{j=i}^N (\mathbf{R}_i - \mathbf{R}_j)^2. \quad (1.19)$$

For polymers the square gyration radius is averaged over the ensemble giving the mean square radius of gyration [1]:

$$\langle R_g^2 \rangle = \frac{1}{N} \sum_{i=1}^N \langle (\mathbf{R}_i - \mathbf{R}_G)^2 \rangle = \frac{1}{N^2} \sum_{i=1}^N \sum_{j=i}^N \langle (\mathbf{R}_i - \mathbf{R}_j)^2 \rangle. \quad (1.20)$$

Radius of gyration of a Gaussian chain for linear polymer is given by [1]

$$R_g = b\sqrt{\frac{N}{6}}. \quad (1.21)$$

1.3 Real Polymer Chains

Until now we were only discussing ideal chain models which do not account for any excluded volume interactions. In reality, however, in many cases these interactions can not be neglected.

The excluded volume represents the effect of the interactions of the segments which are far apart along the chain. Such interactions are called long-range interactions while on contrary interaction among few neighboring segments are called short-ranged interactions. The excluded volume effect was already discussed by Kuhn and then some improvements were initiated by Flory. It shows that long-ranged interactions change the properties of chain entirely. For example $\langle \mathbf{R}_e^2 \rangle$ is no longer proportional to N but to a higher power of N [1-4]

$$\langle \mathbf{R}_e^2 \rangle \propto N^{2\nu} \quad (1.22)$$

where ν is a scaling exponent which will be discussed later in more details.

1.3.1 Excluded Volume Chain Models

In the real chains the nature of excluded volume is quite complicated. The interactions include steric effects, van der Waals attraction and can also involve many other specific interactions. Nevertheless the excluded volume effect is strongly controlled by long-range interactions so the details of the interactions become irrelevant.

Let us define the excluded volume explicitly. The interaction between segments i and j may be expressed as short-ranged function

$$\mathcal{U} = k_B T \tilde{v}(|\mathbf{R}_i - \mathbf{R}_j|) \quad (1.23)$$

where k_B is the Boltzmann constant and T is temperature. This equation can be approximated even further by a delta function [3]

$$\mathcal{U} = k_B T v \delta(|\mathbf{R}_i - \mathbf{R}_j|) \quad (1.24)$$

where v is the excluded volume and has the dimension of volume. The total integration energy can be then written as

$$\mathcal{U} = \frac{1}{2} v k_B T \int_0^N di \int_0^N dj \delta(|\mathbf{R}_i - \mathbf{R}_j|). \quad (1.25)$$

This equation can be then rewritten using the local concentration of segments [3, 4]

$$c(\mathbf{r}) = \sum_i \delta(\mathbf{r} - \mathbf{R}_i) = \int_0^N di \delta(\mathbf{r} - \mathbf{R}_i) \quad (1.26)$$

where \mathbf{r} is a position vector. Rewriting eqn. (1.25) using eqn. (1.26) we get

$$\mathcal{U} = \int d\mathbf{r} \frac{1}{2} v k_B T c(\mathbf{r})^2. \quad (1.27)$$

Using this expression the excluded volume parameter v can be regarded as the virial coefficient between the segments. Further virial coefficient expansion can be done but for swollen chains the density of segments in polymer coil is small and the higher terms can be neglected.

Using mean-field approach internal segment concentration Φ can be defined by replacing average of c^2 by the square of average [4]

$$\langle c^2 \rangle \rightarrow \langle c \rangle^2 \sim \Phi. \quad (1.28)$$

Doing so we ignore all correlations between the segments. The internal segment density is then estimated as [3, 4]

$$\Phi \simeq \frac{N}{\langle R \rangle^3} \propto N^{1-3\nu} = N^{-4/5} \quad \text{for } \nu = 3/5 \quad (1.29)$$

where R is a certain unknown radius (e.g. $R = |\mathbf{R}_e|$). Eqn. (1.29) shows that using above internal segment density Φ becomes very small for large N .

For given combination of polymer and solvent v varies with temperature. More appropriate expression for temperature dependence gives so called Mayer f -function which is defined as the difference between Boltzmann factor for two segments at distance r and two segments at infinite distance ($r = \infty$)

$$f(r) = \exp\left(-\frac{u(r)}{k_B T}\right) - 1. \quad (1.30)$$

The excluded volume v can be then defined as minus the integral of the Mayer f -function over the whole space [1]

$$v = - \int f(r) d\mathbf{r} = \int \left(1 - \exp\left[-\frac{u(r)}{k_B T}\right] \right) d\mathbf{r}. \quad (1.31)$$

This single parameter summarizes the net two body-interaction between monomers.

1.3.2 Flory-Huggins Theory

Here, we describe a mean-field theory of binary mixtures, a Flory-Huggins theory and introduce a Flory interaction parameter. [1] Flory-Huggins theory considers a two-component mixture on lattice with a constant volume where component A occupies a volume fraction ϕ_A and component B occupies a volume fraction ϕ_B . We try to evaluate the energy of mixing \mathcal{U}_{mix} of such system.

The average pairwise interaction of an A-component, \mathcal{U}_A , with one of its neighboring monomers is a volume fraction weighted sum of interaction energies

$$\mathcal{U}_A = u_{AA}\phi_A + u_{AB}\phi_B \quad (1.32)$$

where u_{AA} is interaction energy between components A and A and u_{AB} is interaction energy between component A and B . The corresponding energy of a B-component, \mathcal{U}_B , is

$$\mathcal{U}_B = u_{BB}\phi_B + u_{AB}\phi_A \quad (1.33)$$

where u_{BB} is interaction energy between components B and B . We write the total interaction energy of the mixture, \mathcal{U} , by summing over all interactions

$$\mathcal{U} = \frac{kn}{2} [\mathcal{U}_A\phi_A + \mathcal{U}_B\phi_B] \quad (1.34)$$

where k is number of lattice sites which also gives the number of pairwise interactions per site. Since the total volume stays constant we can rewrite ϕ_B as $\phi_B = 1 - \phi_A$. Substituting that into eqn. (1.34) and using eqns. (1.32) and (1.33) we obtain

$$\mathcal{U} = \frac{kn}{2} [u_{AA}\phi^2 + 2u_{AB}\phi(1 - \phi) + u_{BB}(1 - \phi)^2]. \quad (1.35)$$

Then the total energy of both components before mixing can be expressed as

$$\mathcal{U}_0 = \frac{kn}{2} [u_{AA}\phi + u_{BB}(1 - \phi)]. \quad (1.36)$$

The energy of mixing can be then written as a difference of energies before eqn. (1.34) and after eqn. (1.36) mixing as

$$\mathcal{U} - \mathcal{U}_0 = \frac{kn}{2} \phi(1 - \phi) (2u_{AB} - u_{AA} - u_{BB}). \quad (1.37)$$

It is convenient to study the intensive parameter $\Delta\mathcal{U}_{\text{mix}}$ which is the energy change of mixing per site

$$\Delta\mathcal{U}_{\text{mix}} = \frac{\mathcal{U} - \mathcal{U}_0}{n} = \frac{k}{2} \phi(1 - \phi) (2u_{AB} - u_{AA} - u_{BB}). \quad (1.38)$$

The Flory interaction parameter χ is defined to characterize the difference of interaction energies in the mixture

$$\chi = \frac{k}{2} \frac{2u_{AB} - u_{AA} - u_{BB}}{k_B T}. \quad (1.39)$$

χ is a dimensionless measure of the differences in the strength of the pairwise interaction energies between species in a mixture. Using this parameter energy of mixing per lattice site

$$\Delta \mathcal{U}_{\text{mix}} \Delta \mathcal{U}_{\text{mix}} = \chi \phi (1 - \phi) k_B T. \quad (1.40)$$

This energy is a mean-field description of all binary regular mixtures, regular solutions, polymer solutions as well as polymer blends.

1.3.3 Regimes of Polymer Solutions

Using descriptions of polymer solutions mentioned above various regimes of polymer solutions can be identified. First let us discuss the athermal solvents. For high temperate limit the Mayer f -function has no but contribution from hard core repulsion. The excluded volume becomes independent of temperature at high temperatures, making solvent athermal. We denote the excluded volume at this temperature v_{athermal} .

In athermal limit the monomer makes no energetic distinction between other monomers and solvent. In typical solvent monomer monomer attraction is slightly stronger than the monomer solvent attraction which leads to lower excluded volume than the athermal value

$$0 < v < v_{\text{athermal}}. \quad (1.41)$$

At special temperature called θ or Flory temperature contribution to the excluded volume from hard-core repulsion exactly matches attractive forces and cancels to zero resulting in θ -solvents

$$v = 0, \quad \chi = \frac{1}{2}. \quad (1.42)$$

Ideal chains are describing polymers at this temperature. At temperature below θ -temperatures are called poor solvent. In such solvents the excluded volume is negative.

$$v_{\text{non-solvent}} < v < 0. \quad (1.43)$$

The limiting case of poor solvents is called non-solvent. We denote the excluded volume of non-solvents $v_{\text{non-solvent}}$. [1] Further in this work we will only discuss polymers in good and athermal solvents.

1.3.4 Flory Exponent

Here, we shall derive a Flory arguments for calculating the scaling exponent. The original ideal of Flory was to calculate the coil size as a sum up two effects: a repulsive excluded volume effect swelling the coil as volume interactions of the links, F^{int} , and the elastic energy arising from connectivity of chains, F^{el} , thus [2–4]

$$F = F^{\text{el}} + F^{\text{int}}, \quad (1.44)$$

where F is the free energy. Let us take the free energy of a Gaussian chain whose end-to-end vector \mathbf{R}_e is fixed. Partition function corresponding to a given value of \mathbf{R}_e is $Q(\mathbf{R}_e)$. The free energy of the ideal polymer with the given value \mathbf{R}_e is than given by [3]

$$F^{\text{el}} = -k_B T \ln Q(\mathbf{R}_e, N) + \text{const.} \quad (1.45)$$

For $v = 0$, the free energy F^{el} can obtained using end-to-end vector distribution as [3]

$$F^{\text{el}} = k_B T \frac{3\mathbf{R}_e^2}{2Nb^2} + \text{const.} \quad (1.46)$$

To estimate the effect of the extended volume interaction we disregard the connectivity of chain and calculate the interaction energy of a segment gas confined in a volume R^3 ($R = |\mathbf{R}_e|$). Using the internal segment concentration $\Phi = N/R^3$, the interaction energy is estimated as

$$F^{\text{int}} = vk_B T \Phi^2 R^3, \quad (1.47)$$

thus [3]

$$F = k_B T \left(\frac{3\mathbf{R}_e^2}{2Nb^2} + v \frac{N^2}{R^3} \right). \quad (1.48)$$

The average size can be estimated from value which minimizes F . From $\partial F / \partial R$ we obtain

$$\langle R \rangle \simeq \sqrt{Nb} \left(\frac{\sqrt{N}v}{b^3} \right)^{1/5} \propto N^{3/5}. \quad (1.49)$$

Such calculation gives the scaling exponent $\nu = 3/5$. This result is very close to the experimental value however this description turns out to not be adequate because both the repulsive energy as well as the elastic energy are highly overestimated. The success of Flory calculation comes mainly from cancellation of errors. [4]

1.4 Fluctuation Theory and Scaling Concepts

An analysis of a Gaussian coil shows that low concentration polymer solution in good solvent is a system with strongly correlated fluctuations over long distances. It is obvious that repulsive volume interaction among links can only intensify these fluctuations. Hence, such a system can not be very well described using mean-field approach which is neglecting the fluctuations.

Other physical analogies can be found for system such a polymer in good solvent. For example magnetic system near critical point or second order transition where self-consistent Landau theory does not apply because of the fluctuation grow. Universality of second order phase transition is expressed by independence of so called critical exponents for each specific system from microscopic details of its structure. This critical exponent define the behavior of various physical quantities near a transition point. For polymers as for the magnets the critical exponents are universal, that is independent of specific chemical structure of macromolecules and it is defined only by their most general properties. The essential is that critical parameters and fluctuations behavior of polymer as well as other systems generally depends on dimensional bulk system.

In 1972 P. G. de Gennes pointed out that statistics of single long polymer chain in a good solvent is equivalent to that of a magnet near the second order phase transition point in the limit where the number n of components of an elementary magnetic moment is formally made to approach to zero ($n \rightarrow 0$). The fluctuation theory of second order transitions in magnets have been thoroughly developed and many results in this area could be transferred to polymers using so called $n = 0$ methods. How more accurate results for critical exponent can be obtain we outline in the following text.

1.4.1 Scaling

Let us introduce the scaling in another fashion. Consider a Gaussian chain, as mentioned before its statistical property do not depend on the local structure of the chain. Let us than take apart from the original chain with N segments of bond length b another Gaussian chain of $N' = N/\lambda$ segments with bond length $\sqrt{\lambda}b$. Then the transformation of the old chain to the new one is the change of parameters

$$N \rightarrow N/\lambda, \quad b \rightarrow b\sqrt{\lambda}. \quad (1.50)$$

If you can estimate how the quantity of such transformation changes, you can make some conclusions about dependence of physical quantity on the parameters N and b .

We consider various lengths that characterize the size of a Gaussian chain. For example root of mean square of end-to-end distance $\langle \mathbf{R}_e^2 \rangle^{1/2}$

or radius of gyration R_g . Without any calculations we can see that these quantities are proportional to $\sqrt{\lambda}b$. Let us demonstrate it by following: the average size of polymer has the dimension of length and can be written as

$$\text{average size} = f(N)b. \quad (1.51)$$

The size of the polymer must be invariant under transformation eqn. (1.50)

$$f(N)b = f(N/\lambda)\sqrt{\lambda}b. \quad (1.52)$$

That is satisfied only when

$$f(N)b = \text{const} \times \sqrt{\lambda}b. \quad (1.53)$$

Hence, the distinction among various length is only a numerical constant. Suppose that similar property exist for the excluded volume chain under following transformation:

$$N \rightarrow N/\lambda, \quad b \rightarrow b\lambda^\nu \quad (1.54)$$

where ν is the scaling exponent in $\langle R \rangle \propto N^\nu$. By the same argument as above we can show that average size of the excluded volume chain has following form

$$\text{average size} = \text{const} \times N^\nu b. \quad (1.55)$$

That indicates that there is only one length-scale to characterize the macroscopic size of the polymer chain that is the difference between $\langle R_e^2 \rangle^{1/2}$ and R_g is only a numerical constant

$$R_g = \text{const} \times \langle R_e^2 \rangle^{1/2} \simeq N^\nu b. \quad (1.56)$$

1.4.2 Perturbation Theory

The variety of techniques to evaluate the critical exponent has been developed, few of them we will try to briefly discuss in the following text and try to outline how more precise results for critical exponent can be obtain analytically. First we mention a perturbation theory calculation which can be with advantage applied to system close to θ -point, i.e. is if excluded volume v is small. [2,3] Hence, $\langle R_e \rangle$ can be calculated as a power expansion of v similarly as perturbation theory virial expansion is used in imperfect gas. Trough straightforward, such a calculation becomes quite tedious and we shall not show it here. The perturbation calculation gives [3]

$$\begin{aligned} \langle R_e \rangle = Nb^2 & \left(1 + \frac{3}{4}z - 2.075z^2 + 6.297z^3 - 25.057z^4 \right. \\ & \left. + 116.135z^5 - 594717z^6 + \dots \right), \end{aligned} \quad (1.57)$$

where z is defined as

$$z = \left(\frac{3}{2\pi} \right) \frac{v\sqrt{N}}{b^3}. \quad (1.58)$$

You can note that z is proportional to \sqrt{N} thus the perturbation expansion becomes useless for large N . However, it has been shown that the series in eqn. (1.57) is asymptotic and by appropriate resummation technique (e.g. Borel transforms [5,6]) the exponent ν can be estimated as $\nu = 0.588 \pm 0.001$.

1.4.3 Renormalization Group Theory

Another way to estimate the scaling exponent is to use renormalization group technique which was developed to study the critical phenomena. It was originally invented by Wilson and to polymers it was first applied by de Gennes and des Cloizeaux. [4] The calculation method of the renormalization group theory is quite complex and has many variations. [7,8] We mention the ϵ -expansion scheme. It is possible to develop an expansion scheme regarding $\epsilon = 4 - d$ as an expansion parameter. [2] Such scheme gives

$$\nu = \frac{1}{2} \left(1 + \frac{1}{8}\epsilon + \frac{15}{256}\epsilon^2 \right). \quad (1.59)$$

For $d = 3$ this gives $\nu = 0.592$ which compares well with more accurate result $\nu = 0.588$.

1.5 Dynamical Properties

Here, we discuss some dynamical properties of polymer solutions. We only briefly mention the Rouse model and then concentrate on Zimm model and how it can be used to estimate hydrodynamic radius, R_h , of a polymer. In following derivations we closely follow the textbook of Doi [3]. The static properties are described by a set of beads connected along the chain. So it seems natural to describe the polymer dynamics as Brownian motion of such beads. Such scheme was proposed by Rouse.

1.5.1 Rouse Model

Let us have a set of beads $\{R_i\} \equiv (R_1, R_2, \dots, R_i)$. In the Rouse model on each bead act three following forces: first force from neighboring bead $f^{(p)}$, force of friction against solvent $f^{(fr)}$ and then a random force $f^{(rnd)}$. Equation of motion of i -th bead can be written as [2]

$$m \frac{\partial^2 \mathbf{R}_i}{\partial t^2} = f_i^{(p)} + f_i^{(fr)} + f_i^{(rnd)}. \quad (1.60)$$

We write equation of motion of Brownian particle in Langevin form as [3]

$$\zeta \frac{dx}{dt} = -\frac{\partial \mathcal{U}}{\partial x} + f(t) \quad (1.61)$$

where $f(t)$ is a random force, ζ is a friction coefficient and its inverse $1/\zeta$ is called the mobility. If particle is sufficiently large, ζ can be obtained from hydrodynamics. For example if the particle is a sphere of radius a and viscosity of solvent is η_s than

$$\zeta = 6\pi\eta_s a. \quad (1.62)$$

Eqn. (1.60) can be rewritten using the Langevin form equation corresponding to Smoluchowski equation in multidimensional space as [3]

$$\frac{\partial}{\partial t} \mathbf{R}_i(t) = \sum_j \mathbf{H}_{ij} \left(-\frac{\partial \mathcal{U}}{\partial \mathbf{R}_j} + \mathbf{f}_j(t) \right) + \frac{1}{2} k_B T \sum_j \frac{\partial}{\partial \mathbf{R}_j} \mathbf{H}_{ij} \quad (1.63)$$

where \mathcal{U} is potential and \mathbf{H} is a mobility matrix. In Rouse model the excluded volume interaction and hydrodynamic interaction are neglected and mobility tensor and interaction potential are described as [3]

$$\mathbf{H}_{ij} = \frac{\mathbf{I}}{\zeta} \delta_{ij} \quad (1.64)$$

and potential in θ -condition is written as

$$\mathcal{U} = \frac{k}{2} \sum_{i=2}^N (\mathbf{R}_i - \mathbf{R}_{i-1})^2 \quad (1.65)$$

where δ_{ij} is Kronecker delta and

$$k = \frac{3k_B T}{b^2}. \quad (1.66)$$

However neglecting the hydrodynamic interaction turns out to be crucial and Rouse model does not give correct results. Even though this model is quite important we will not discuss it here any more. Details on Rouse model can reader easily find elsewhere. [2, 3]

1.5.2 Zimm model

To describe the polymer dynamics in dilute solutions we have taken the hydrodynamic interaction into account. A way to do that was proposed by Zimm and shall discuss it now. Zimm expressed the mobility matrix as follows [3]

$$\mathbf{H}_{ii} = \frac{\mathbf{I}}{\zeta}, \quad (1.67)$$

$$\mathbf{H}_{ij} = \frac{1}{8\pi\eta_s|\mathbf{r}_{ij}|}(\hat{\mathbf{r}}_{ij} \otimes \hat{\mathbf{r}}_{ij} + \mathbf{I}) \quad \text{for } i \neq j \quad (1.68)$$

where $\mathbf{r}_{ij} \equiv \mathbf{R}_i - \mathbf{R}_j$ and $\hat{\mathbf{r}}_{ij}$ is the unit vector in direction of \mathbf{r}_{ij} and \mathbf{I} is a unit matrix. For that tensor is be shown that [3]

$$\frac{\partial}{\partial \mathbf{R}_i} \mathbf{H}_{ij} = 0. \quad (1.69)$$

The Langevin equation (1.63) thus becomes

$$\frac{\partial}{\partial t} \mathbf{R}_i = \sum_{ij} \mathbf{H}_{ij} \left(-\frac{\partial \mathcal{U}}{\partial \mathbf{R}_j} + \mathbf{f}_j(t) \right). \quad (1.70)$$

For θ condition eqn. (1.65) and eqn. (1.70) give in continuous limit [3]

$$\frac{\partial}{\partial t} \mathbf{R}_i = \sum_{ij} \mathbf{H}_{ij} \left(k \frac{\partial^2}{\partial j^2} \mathbf{R}_j + \mathbf{f}_j(t) \right). \quad (1.71)$$

\mathbf{H}_{ij} is, however, nonlinear function of \mathbf{r}_{ij} and eqn. (1.71) is quite difficult to handle. Zimm introduced the preaveraging approximation, which replaces \mathbf{H}_{ij} by its average to simplify the analysis. [3]

$$\mathbf{H}_{ij} \rightarrow \langle \mathbf{H}_{ij} \rangle = \int d\{\mathbf{R}_i\} \mathbf{H}_{ij} \Psi(\{\mathbf{R}_i\}, t) \quad (1.72)$$

where Ψ is a distribution function. Considering problems near equilibrium, we may use the equilibrium distribution function in the average of eqn. (1.72)

$$\mathbf{H}_{ij} \rightarrow \langle \mathbf{H}_{ij} \rangle_{\text{eq}} = \int d\{\mathbf{R}_i\} \mathbf{H}_{ij} \Psi_{\text{eq}}(\{\mathbf{R}_i\}). \quad (1.73)$$

Distribution \mathbf{r}_{ij} is independent of $|\mathbf{r}_{ij}|$, so $\langle \mathbf{H}_{ij} \rangle_{\text{eq}}$ can be written as

$$\langle \mathbf{H}_{ij} \rangle_{\text{eq}} = \frac{1}{8\pi\eta_s} \left\langle \frac{1}{|\mathbf{r}_{ij}|} \right\rangle_{\text{eq}} \langle \hat{\mathbf{r}}_{ij} \otimes \hat{\mathbf{r}}_{ij} + \mathbf{I} \rangle_{\text{eq}}. \quad (1.74)$$

Using

$$\langle \hat{\mathbf{r}}_{ij} \otimes \hat{\mathbf{r}}_{ij} \rangle = \frac{\mathbf{I}}{3} \quad (1.75)$$

we have

$$\langle \mathbf{H}_{ij} \rangle = \frac{\mathbf{I}}{6\pi\eta_s} \left\langle \frac{1}{|\mathbf{R}_i - \mathbf{R}_j|} \right\rangle. \quad (1.76)$$

In preaveraging approximation eqn. (1.70) thus becomes

$$\frac{\partial}{\partial t} \mathbf{R}_i(t) \sum_j \frac{\mathbf{I}}{6\pi\eta_s} \left\langle \frac{1}{|\mathbf{R}_i - \mathbf{R}_j|} \right\rangle \left(k \frac{\partial^2}{\partial j^2} \mathbf{R}_j(t) + \mathbf{f}_j(t) \right). \quad (1.77)$$

This approximation might seem quite crude, however, the results it gives have been shown to not be very different from those of more sophisticated calculations. To analyze eqn. (1.77) we rewrite it in term of Rouse normal coordinates \mathbf{X}_p . [2, 3]

$$\frac{\partial}{\partial t} \mathbf{X}_p = \sum_q h_{pq} (-k_q \mathbf{X}_q + \mathbf{f}_q) \quad (1.78)$$

where

$$\mathbf{X}_p \equiv \frac{1}{N} \int_0^N di \cos\left(\frac{\pi p i}{N}\right) \mathbf{R}_i(t) \quad \text{where } p = 0, 1, 2, \dots \quad (1.79)$$

$$k_p = \frac{2\pi^2 k}{N} p^2 = \frac{6\pi^2 k_B T}{Nb^2} p^2 \quad (1.80)$$

and

$$h_{pq} = \frac{1}{N^2} \int_0^N di \int_0^N dj \cos\left(\frac{\pi p i}{N}\right) \cos\left(\frac{\pi q j}{N}\right) \frac{\mathbf{I}}{6\pi\eta_s} \left\langle \frac{1}{|\mathbf{R}_i - \mathbf{R}_j|} \right\rangle. \quad (1.81)$$

h_{pq} is nearly diagonal and by neglecting off-diagonal components and we get so called Kirkwood-Riseman approximation [2]

$$h_{pq} \simeq h_{qq} \delta_{pq}. \quad (1.82)$$

It gives

$$\zeta_p \frac{\partial}{\partial t} \mathbf{X}_p(t) = -k_p \mathbf{X}_p + \mathbf{f}_p(t) \quad (1.83)$$

$$\zeta_p = (h_{pp})^{-1} = \left[\frac{1}{N^2} \int_0^N di \int_0^N dj \cos\left(\frac{\pi p i}{N}\right) \cos\left(\frac{\pi q j}{N}\right) \times \right. \\ \left. \times \frac{1}{6\pi\eta_s} \left\langle \frac{1}{|\mathbf{R}_i - \mathbf{R}_j|} \right\rangle \right]^{-1}. \quad (1.84)$$

For $p = 0$ it gives the result for so called non-draining limit immediately.

$$\zeta_0 = (h_{00})^{-1} = 6\pi\eta_s N^2 \left[\sum_n \sum_m \left\langle \frac{1}{|\mathbf{R}_n - \mathbf{R}_m|} \right\rangle \right]^{-1}. \quad (1.85)$$

1.5.3 Hydrodynamic Radius

Hydrodynamic radius is a radius of a hard sphere that diffuses at the same rate as the polymer molecule. In the non-draining limit, the friction coefficient, ζ , can be expressed as

$$\zeta = \frac{3\pi\eta_s N^2}{\sum_i \sum_{j>i} \langle \mathbf{r}_{ij}^{-1} \rangle} \quad (1.86)$$

where $\langle \mathbf{r}_{ij}^{-1} \rangle$ denotes the average over all conformations and η_0 denotes the viscosity of the solvent. Friction coefficient and hydrodynamic radius, R_h are related via

$$\langle R_h \rangle = \frac{\zeta}{6\pi\eta_0} = \frac{N^2}{2 \sum_i \sum_{j>i} \langle \mathbf{r}_{ij}^{-1} \rangle}. \quad (1.87)$$

Simulation time of calculation of R_h according to eqn. (1.87) scales with N^2 . In order to save computational time we calculate only an estimate of R_h . Upon reversing the order of averaging, we replace the exact average over double sum by average over N randomly chosen inter mass point distances \mathbf{r}_{ij} . Thus [9]

$$\frac{2 \sum_i \sum_{j>i} \langle \mathbf{r}_{ij}^{-1} \rangle}{N^2} = \frac{\left\langle 2 \sum_i \sum_{j>i} \mathbf{r}_{ij}^{-1} \right\rangle}{N^2} \approx \frac{\left\langle \sum_{k=1}^N \mathbf{r}_{i(k)j(k)}^{-1} \right\rangle}{N}. \quad (1.88)$$

CHAPTER 2

Monte Carlo

In this work the Monte Carlo methods are crucial. We devote this chapter to them. Monte Carlo methods are stochastic techniques often used for simulating physical, chemical or mathematical systems. It was developed by von Neumann, Ulam, Metropolis and others in the 1940s. [10–12] They realized that determinate mathematical problems can be treated by finding a probabilistic analog which can be solved by a stochastic sampling experiment. Such experiment is described in following section and it is shown on Figure 2.1. Treating simple problems this is probably not the method of choice, however, we will see that while dealing with more complex systems this technique is very powerful and efficient.

In the following text we try to describe basic principles of Monte Carlo methods. Then we focus on Monte Carlo techniques we use in our simulations.

2.1 Monte Carlo Integration

To demonstrate the very basics of Monte Carlo we begin with simple Monte Carlo integration, that is a random number sampling experiment. [10] Let X_1, X_2, \dots, X_N be random variables with probability distribution $f(x)$ and then for function $g(x)$ let G_N be an estimator

$$G_N = \frac{1}{N} \sum_{i=1}^N g(X_i). \quad (2.1)$$

Then

$$\langle G_N \rangle = \int_{-\infty}^{\infty} f(x)g(x)dx, \quad (2.2)$$

and

$$\text{var}(G_N) = \frac{1}{N} \text{var}(g) \quad (2.3)$$

As $N \rightarrow \infty$ and if the variance exists, the distribution of possible values of G_N narrows about the mean as $N^{-\frac{1}{2}}$ or in other words the probability of finding G_N at some fixed distance away from $\langle G_N \rangle$ becomes smaller.

Usually, the basic random variable used in Monte Carlo is distributed uniformly between 0 and 1. [13]

$$f_{\text{rnd}}(x) = 1, \quad 0 \leq x \leq 1. \quad (2.4)$$

To illustrate let us show how a simple Monte Carlo integration can be used to evaluate number π (Figure 2.1). [10]

Consider the unit square in the plane xy and the circle with unit radius. Integrating over the unit circle but counting only those pairs of x and y that lie within quarter circle yields the area of the quarter circle. That is

$$\int_0^1 \int_0^1 f(x, y) g(x, y) dx dy = \frac{\pi}{4} \quad (2.5)$$

where

$$f(x, y) = \begin{cases} 1 & (x, y) \in (0, 1) \otimes (0, 1) \quad (\text{i.e. inside the unit square}) \\ 0 & \text{otherwise} \end{cases} \quad (2.6)$$

and

$$g(x, y) = \begin{cases} 1 & x^2 + y^2 \leq 1 \\ 0 & x^2 + y^2 > 1. \end{cases} \quad (2.7)$$

Since x and y are independent,

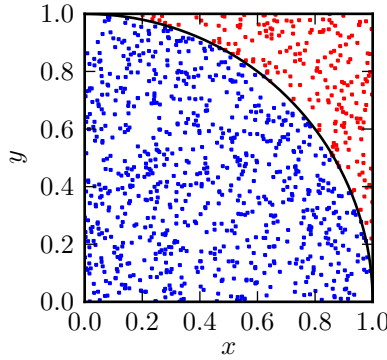
$$f(x, y) = f_{\text{rnd}}(x) f_{\text{rnd}}(y). \quad (2.8)$$

2.2 The Metropolis Method

Having introduced simple Monte Carlo integration, we proceed to more advanced sampling technique. Consider a hard sphere fluid of N particles and let us denote Z to be configurational part of a partition function [11, 12]

$$Z \equiv \int d\mathbf{r}^N \exp [-\beta \mathcal{U}(\mathbf{r}^N)] \quad (2.9)$$

where \mathcal{U} is potential and \mathbf{r}^N stands for the coordinates of all N particles. Using simple Monte Carlo integration to evaluate this integral we would,

Figure 2.1: Monte Carlo integration

however, find out that for overwhelming number of points the Boltzmann factor is vanishingly small because for more dense system it is very difficult to generate configurations where spheres do not overlap, meaning that their Boltzmann factor is non-zero.

Fortunately, we are rather than in evaluating configurational part of partition function itself interested in evaluating averages such as

$$\langle A \rangle = \frac{\int d\mathbf{r}^N A(\mathbf{r}^N) \exp[-\beta\mathcal{U}(\mathbf{r}^N)]}{\int d\mathbf{r}^N \exp[-\beta\mathcal{U}(\mathbf{r}^N)]}. \quad (2.10)$$

In such case we can reduce the problem only to evaluating the ratio of these integrals. In 1953 Metropolis *et al.* [14] showed that it is possible to derive an efficient Monte Carlo scheme to sample such a ratio. The ratio $\exp[-\beta\mathcal{U}(\mathbf{r}^N)]/Z$ in eqn. (2.10) is then probability density of finding the system around the configuration \mathbf{r}^N . Let us denote this probability density by

$$\mathcal{N}(\mathbf{r}^N) \equiv \frac{\exp[-\beta\mathcal{U}(\mathbf{r}^N)]}{Z}. \quad (2.11)$$

Now, let us imagine that we are able to somehow randomly generate points in configurational space so they have the probability distribution $\mathcal{N}(\mathbf{r}^N)$. Then, clearly, the number of points n_i generated per unit volume around a point \mathbf{r}^N is equal to $\mathcal{L}\mathcal{N}(\mathbf{r}^N)$ where \mathcal{L} is total number of generated points. So

$$\langle A \rangle \approx \frac{1}{\mathcal{L}} \sum_{i=0}^{\mathcal{L}} n_i A(\mathbf{r}_i^N). \quad (2.12)$$

We should note that using this approach we only know the Boltzmann factor, $\exp[-\beta\mathcal{U}(\mathbf{r}^N)]$, and not the configurational part of partition function, Z , thus we do not know the absolute but only the relative probability of visiting points in configurational space.

Let us derive the Metropolis scheme to show how to generate points in configurational space with desired distribution, in our case, Boltzmann distribution \mathcal{N} .

The general approach uses a Markov chain which is a special case of Markov process. Markov chain $\mathbf{X} = \{X_0, X_1, \dots\}$ is a particular type of a stochastic process taking at times $k \in \mathbb{Z}_+$, values X_k in a state space \mathcal{S} with Markov property defined as [15]

$$P(X_{k+1} = x | X_1 = x_1, X_2 = x_2, \dots, X_k = x_k) = P(X_{k+1} = x | X_k = x_k). \quad (2.13)$$

Let us take the state space to be finite and $\{A_i\} \in \mathcal{S}, i = 1, 2, \dots, M$. The probability of transition from the state i to the state j at time k for time-homogeneous Markov chain we define as

$$P_{j|i} = P(X_{k+1} = j | X_k = i) \quad (2.14)$$

so transition from i to j at time k can be written as

$$P_j^{(k+1)} = \sum_{i=1}^M P_i^{(k)} P_{j|i}. \quad (2.15)$$

This can be rewritten using the transition or stochastic matrix $\boldsymbol{\pi}$ as [12]

$$\boldsymbol{\rho}^{(k+1)} = \boldsymbol{\rho}^{(k)} \boldsymbol{\pi} \quad (2.16)$$

where $P_i^{(k)}$ is the probability of state i at time k and $\boldsymbol{\rho}^{(k)}$ is stochastic vector at time k and sum over state j gives

$$\sum_j^M P_{j|i} = 1. \quad (2.17)$$

It is possible to calculate the limiting distribution as [12]

$$\boldsymbol{\rho} = \lim_{k \rightarrow \infty} \boldsymbol{\rho}^{(1)} \boldsymbol{\pi}^{(k)} \quad (2.18)$$

for given transition matrix, where $\boldsymbol{\rho}^{(1)}$ is initial stochastic vector. From eqn. (2.18) it is clear that limiting distribution $\boldsymbol{\rho}$ must satisfy eigenvalue equation

$$\boldsymbol{\rho} \boldsymbol{\pi} = \boldsymbol{\rho}. \quad (2.19)$$

That is a matrix of an irreducible chain. Irreducible or ergodic chain is a one where every state can be reached from another one. A suitable scheme

was derived by Metropolis. It is often known as asymmetrical solution. If ($i \neq j$) this solution considers two cases [11, 12]

$$P_{j|i} \geq 0 \quad \forall \quad i, j = 1, \dots, M \quad (2.20)$$

$$\sum_{j=1}^M P_{j|i} = 1 \quad \forall \quad i, j = 1, \dots, M \quad (2.21)$$

$$\rho \pi = \rho. \quad (2.22)$$

Next to help us find a solution we replace detail balance condition by unnecessary condition of microscopic reversibility

$$P_i P_{j|i} = P_j P_{i|j}. \quad (2.23)$$

Summing over all states i we gain

$$\sum_i P_i P_{j|i} = \sum_i P_j P_{i|j} = P_j \sum_i P_{i|j} = P_j. \quad (2.24)$$

These equation do specify transition matrix. Let us take

$$P_i = \frac{\exp(-\beta \mathcal{U}_i)}{Q} \quad (2.25)$$

than substituting it into eqn. (2.24) we get

$$\frac{P_{i|j}}{P_{j|i}} = \frac{P_i}{P_j} = \exp[-\beta(\mathcal{U}_i - \mathcal{U}_j)] \quad (2.26)$$

or

$$P_{i|j} = P_{j|i} = 0. \quad (2.27)$$

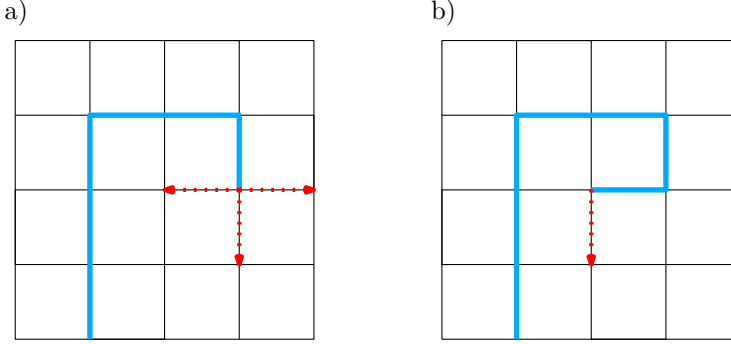
In general case this result means that it is sufficient that we have relative probabilities. The transition matrix is define by [11, 12]

$$P_{j|i} = \begin{cases} \alpha_{j|i} & \text{for } i \neq j \text{ and } P_j \geq P_i \\ \alpha_{j|i} \frac{P_j}{P_i} & \text{for } i \neq j \text{ and } P_j < P_i \\ 1 - \sum_{i \neq j} P_{j|i} & \text{for } i = j \end{cases} \quad (2.28)$$

where $\alpha_{j|i}$ is any stochastic matrix and fulfill condition of microscopic reversibility. This is the matrix suggested by Metropolis. The first two rows are usually rewritten as

$$P_{j|i} = \alpha_{j|i} \min \left\{ 1, \frac{P_j}{P_i} \right\} \quad \text{for } i \neq j. \quad (2.29)$$

At this point it should be stressed that using this scheme we introduce a bias into our computations and the generated samples become highly correlated. This we will discuss in next chapter.

Figure 2.2: Rosenbluth scheme

2.3 The Rosenbluth & Rosenbluth Method

Various schemes how to generate self-avoiding walks (SAW) on lattice and also off-lattice were developed by various authors. In following we describe Rosenbluth and Rosenbluth (RR) scheme which we adopt for our calculation. RR scheme was originally developed to effectively simulate polymer on lattice in good solvent but it can be easily extended to off-lattice case as well. [11]

First, we show how standard Metropolis scheme would be used and then we proceed to RR scheme. Let us consider a chain of N segments on cubic lattice. Using a classical Metropolis scheme we insert first segment and then all following segments we insert to any of its k neighboring lattice sites (for cubic lattice $k = 6$). Doing so we can by incorporating Metropolis scheme sample all the chains with correct probability. However, if chosen site is already occupied the chain intersects itself and generated conformation is to be rejected. This show out to be crucial and the algorithm becomes very inefficient for large N .

In 1955 Rosenbluth and Rosenbluth proposed a scheme to sample more efficiently. [16] Using this RR scheme instead of choosing the direction at random favoring the direction with the highest Boltzmann factor. Yet, doing so we introduce a bias in our computation and we must introduce a correction for that.

In following, we describe the Rosenbluth algorithm and show it gives correct average having Boltzmann distribution. [11] Let interaction energy of i -th segment of chain n to be denoted by $u^{(i)}(n)$. We insert the first monomer and we denote its energy by $u^{(1)}(n)$. Let the RR weight of this monomer be defined as

$$w_1 = k \exp \left[-\beta u^{(1)}(n) \right]. \quad (2.30)$$

Building following segments we define the j -th segment trial position to have the energy $u^{(i)}(j)$. From k possibilities we select one according to probability

$$p^{(i)}(n) = \frac{\exp[-\beta u^{(i)}(n)]}{w_i} \quad (2.31)$$

where w_i is defined as

$$w_i = \sum_{j=1}^k \exp[-\beta u^{(i)}(j)] \quad (2.32)$$

Interaction energy $u^{(i)}(j)$ includes interaction of segment l_i with other molecules and with segments l_1 up to l_{i-1} of the same macromolecule. The interaction energy of whole chain n is

$$\mathcal{U}(n) = \sum_{i=1}^N u^{(i)}(n). \quad (2.33)$$

The normalized RR factor of configuration n is

$$\mathcal{W}(n) = \prod_{i=1}^N \frac{w_i(n)}{k}. \quad (2.34)$$

In case of athermal solvent we do not include energies and the RR weight reduces simply to

$$w_i = \frac{k_i}{k} \quad (2.35)$$

and the RR factor of configuration n is than

$$\mathcal{W}(n) = \prod_{i=1}^N w_i. \quad (2.36)$$

Eqn. (2.12) becomes

$$\langle A \rangle_{\mathcal{R}} = \frac{\sum_{n=1}^{\mathcal{M}} \mathcal{W}(n) A(n)}{\sum_{n=1}^{\mathcal{M}} \mathcal{W}(n)} \quad (2.37)$$

where \mathcal{M} is number of generated chains and $\langle \dots \rangle_{\mathcal{R}}$ indicates that conformations have been generated using Rosenbluth scheme. Probability of generation a particular conformation n is given by using equation () and ()

$$\mathcal{P}(n) = \prod_{i=1}^N \frac{\exp[-\beta u^{(i)}(n)]}{w_i(n)} = \frac{k^N \exp[-\beta \mathcal{U}(n)]}{\mathcal{W}(n)}. \quad (2.38)$$

It should be noted that probability is normalized

$$\sum_n \mathcal{P}(n) = 1. \quad (2.39)$$

Let us show that using RR scheme we will get a proper average.

$$\langle A \rangle_{\mathcal{R}} = \frac{\sum_{n=1}^{\mathcal{M}} \mathcal{W}(n) A(n) \mathcal{P}(n)}{\sum_{n=1}^{\mathcal{M}} \mathcal{W}(n) \mathcal{P}(n)} \quad (2.40)$$

Substituting (2.34) into (2.38) we get

$$\begin{aligned} \langle A \rangle_{\mathcal{R}} &= \frac{\sum_{n=1}^{\mathcal{M}} \mathcal{W}(n) A(n) \prod_{i=1}^N \exp[-\beta u^{(i)}(n)] / w_i(n)}{\sum_{n=1}^{\mathcal{M}} \mathcal{W}(n) \prod_{i=1}^N \exp[-\beta u^{(i)}(n)] / w_i(n)} \\ &= \frac{\sum_{n=1}^{\mathcal{M}} \mathcal{W}(n) k^N A(n) \exp[-\beta \mathcal{U}(n)] / \mathcal{W}(n)}{\sum_{n=1}^{\mathcal{M}} \mathcal{W}(n) k^N \exp[-\beta \mathcal{U}(n)] / \mathcal{W}(n)} \\ &= \frac{\sum_{n=1}^{\mathcal{M}} A(n) \exp[-\beta \mathcal{U}(n)]}{\sum_{n=1}^{\mathcal{M}} \exp[-\beta \mathcal{U}(n)]} \\ &= \langle A \rangle \end{aligned} \quad (2.41)$$

As we can see RR scheme gives proper average. At the end we can conclude that this scheme gives major improvement and allow us to simulate chains with much larger N but the computational cost still grows exponentially because of the self-trapping. That means that in all surrounding lattice points there is a segment already present. [11]

CHAPTER 3

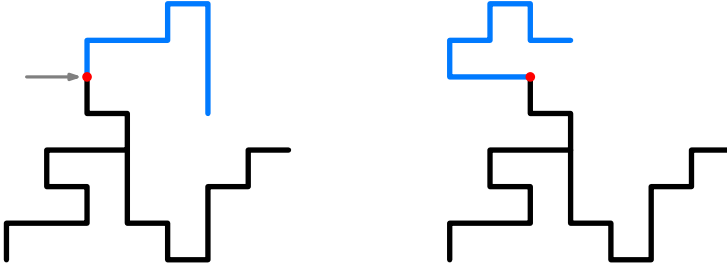
Monte Carlo Calculations

The general description of Monte Carlo methods have been already discussed in previous chapter. In this chapter we present details on how Monte Carlo calculation have been performed. First we discuss the implementation of the RR algorithm we use and we discuss its efficiency, then we show that R_g generated for different architectures follows a proper scaling and how other characteristic, in particular distribution coefficient and depletion layer, can be calculated using conformation obtained from MC simulations.

3.1 Algorithm Implementation

First, we refer to standard RR scheme mentioned in the previous chapter (Section 2.3). Our task is to generate SAWs representing branched polymers with various architectures. As we mentioned already, the RR algorithm remarkably improves the efficiency of generating SAWs but nevertheless the sample attrition still stays exponential because of the self-trapping even though at much slower rate. [11, 17] It is clear, that this self-trapping can be only intensified if we generate a branched polymers which are, from their nature, more dense than the linear ones.

The principle of the technique we use to generate SAWs is rather simple, even though its implementation becomes more complicated from programming point of view. The implementation of the algorithm we use to achieve higher efficiency is following: We start with standard RR scheme and we use it to produce first conformation, but other schemes can be used at this point as well (e.g. the dimerization algorithm which would give us a conformation from correct distribution and thus you could start to sample immediately). At the second step modified RR is already used. Instead of rebuilding entire chain again we chose randomly any point along the chain and then we randomly chose a direction in which we dissolve the rest of the chain from the chosen point. While dissolving this part we have to calculate its RR

Figure 3.1: Monte Carlo step

weight. Then we regrow the dissolved part and we again calculate its RR weight. Doing so a new conformation is created. The new conformation is accepted or rejected according to to Metropolis criteria eqn. (2.29) using calculated weights of dissolved and regrown parts of the chain. A scheme of a modified RR MC step is depicted on the Figure 3.1. The computational time of generation of SAWs still grows exponentially with N but we achieved to reduce the self-trapping so the exponential grow is slower and we improve the algorithm efficiency. [17]

To give some idea about efficiency of this algorithm let as mention following: For example to generate 1000 segments chain about 10^6 independent conformations are needed to calculate an average within 1% error and it takes about 12 hours but to calculate a chain of 2000 segments within this error takes already several days. We found 12 hours calculation reasonable so many of the following SAWs calculations presented have about 1000 segments.

3.1.1 Remark on Bracket Notation

There is a very simple way how trees can be represented using a bracket notation. [18] We adopted this because it allows us to build any given tree recursively, that is in a very simple way. It is however useful not only for programming. In following text we shall use it to describe various architectures presented. This notation uses nested parentheses to describe which points are either disjoint or one contains to the other, parentheses behind a number (number of segments of linear chain) signifies another chain connected to it. The best way to explain is probably an example. For example a star with arms of 100 segments has notation:

$$[100[100][100]] \quad (3.1)$$

to the end of first 100 segments are connected two chains of 100 segments.

3.2 Calculation of Averages

As we mentioned before, configurations obtained from MC are highly correlated. In the following, we explain how we decorrelate our data and how averages and standard deviations are estimated. Also certain number of conformations from the beginning of the simulation has to be left out from the computation of averages since the first conformation is not generated from the correct Boltzmann distribution.

3.2.1 Autocorrelation Function

Let X_1, \dots, X_n be the result of n consecutive measurements. The sample mean we define as

$$\bar{X} \equiv \frac{1}{n} \sum_{t=1}^n X_t \quad (3.2)$$

and variance of correlated values we estimate as [11]

$$\text{var}(\bar{X}) = \langle \bar{X}^2 \rangle - \langle \bar{X} \rangle^2 = \frac{1}{n^2} \sum_{i,j=1}^n \gamma_{ij}, \quad (3.3)$$

$$= \frac{1}{n} \left(\gamma_0 + 2 \sum_{t=1}^{n-1} \left(1 - \frac{t}{n} \right) \gamma_t \right) \quad (3.4)$$

where γ_{ij} is autocorrelation function

$$\gamma_{ij} \equiv \langle X_i X_j \rangle - \langle X_i \rangle \langle X_j \rangle. \quad (3.5)$$

Autocorrelation function is invariant under time translations and depends only on interval $|i - j|$. We, hence, define

$$\gamma_t \equiv \gamma_{ij} \quad \text{where} \quad t = |i - j|. \quad (3.6)$$

For large values of t autocorrelation function decays exponentially. Therefore we define exponential autocorrelation time [17]

$$\tau_{\text{exp},A} = \lim_{t \rightarrow \infty} \frac{t}{-\log \gamma_t}. \quad (3.7)$$

This can be interpreted as relaxation time of the system. In other words it says how many steps is needed before correlation decreases to $1/e$. In our simulations we always leave out at least ten times this autocorrelation time from the beginning of the average evaluation. Then we consider the conformation to have the correct Boltzmann distribution. On the other hand, we define also the integrated autocorrelation time [17]

$$\tau_{\text{int},A} = \frac{1}{2} + \sum_{t=1}^{\infty} \frac{\gamma_t}{\gamma_0}. \quad (3.8)$$

By using it, variance can be estimated more precisely as [17, 19]

$$\text{var}(\bar{X}) \approx \frac{1}{n} 2\tau_{\text{int},A} \gamma_0 \quad \text{for } n \gg \tau. \quad (3.9)$$

This result displays that the variance of \bar{X} is a factor $2\tau_{\text{int},A}$ larger than it would be if the X_1, \dots, X_n were statistically independent.

3.2.2 Block Method

To calculate variance of independent samples we use another alternative method. [19] This method does not use the autocorrelation function to calculate the variance but it uses repeatedly a block transformation

$$X'_i = \frac{1}{2}(X_i + X_{i+1}). \quad (3.10)$$

From original n values of X we obtain $n' = n/2$ new values $X'_1, X'_2, \dots, X'_{n/2}$. The mean value and the variance are invariant under this transformation and it is possible to show that value of γ_0 transforms as

$$\gamma'_0 = \frac{1}{2}(\gamma_0 + \gamma_1). \quad (3.11)$$

From eqn. (3.4) variance is

$$\text{var}(X) \geq \frac{\gamma_0}{n}. \quad (3.12)$$

Value γ_0/n grows after each block transform until γ_1 is not zero. Then γ_0/n is independent under the blocking. And block transformation has a fixed point with $\text{var}(\bar{X}) = \gamma_0/n$ and $\gamma_t = 0$ for $t > 0$. We continue with blocking until $n' = 2$ and for each block transform $\text{var}(\bar{X})$ is calculated

$$\text{var}(X) \approx \frac{c_0}{n' - 1} \quad (3.13)$$

where c_t is an estimator for γ_{ij} , c_0 is of course c_t for $t = 0$,

$$c_t \equiv \frac{1}{n-t} \sum_{k=1}^{n-t} (X_k - \bar{X})(X_{k+t} - \bar{X}). \quad (3.14)$$

Plateau of the value $\text{var}(\bar{X})$ tells us that we reached a stationary point. Then Blocked values are independent and their variance can be estimated. [11]

$$\text{var}(\bar{X}) \approx \frac{c'_0}{n' - 1} \pm \sqrt{\frac{2}{n' + 1} \frac{c'_0}{n' - 1}}. \quad (3.15)$$

3.3 Scaling

In this section we present scaling for various architectures. We would like to stress that main aim of this is rather to validate reliability of the program we developed then to study the scaling behavior. We present our calculations of following architectures: linear, 3-arm star and 6-arm star and asymmetric star ($[N/2[N/4][N/4]]$). We generated SAWs up to 1000 segments for different architectures. Around 10^6 independent conformations is generated for computing the averages and all averages are calculated within 1% error. In Figure 3.2 we show scaling of $\langle R_g^2 \rangle$ for linear chain and in Figure 3.3 we show the scaling of $\langle R_g^2 \rangle$ for all architectures named above. For linear chain The scaling is found as

$$\langle R_g^2 \rangle = AN^{2\nu}. \quad (3.16)$$

The scaling exponents ν and preexponential constant A for Figure 3.3 are in Table 3.3. For stars as well as for linear chains the scaling obtained analytically [20]

$$\langle R_g^2 \rangle = Af^{1-\nu}N^{2\nu}. \quad (3.17)$$

where f in number of arms. This scaling is however supposed to be valid for many arm star with arms of infinite length which is not the case of stars we calculated.

We should discuss the results of scaling in comparison to analytical result, which is $\nu = 0.588$, discussed in Section 1.3. MC and analytical results although close do not exactly match. The reason for the deviation is that analytical methods calculate the scaling at the limit for $N \rightarrow \infty$ while our MC calculations of SAWs have rather small amount of segments $N \sim 1000$. It have been shown that to get agreement on third digit, SAWs of 10000 segments have to be used to evaluate scaling. [21] We would like to point out that all different architectures follow the same scaling exponent ν . The preexponential constant A varies for different architecture and varies also with different models being used.

Table 3.1: Scaling exponents ν and preexponential factors A for different architectures.

Architecture	A	ν
linear	0.175	0.594
3-arm star	0.131	0.596
6-arm star	0.074	0.596
asymmetric star	0.145	0.593

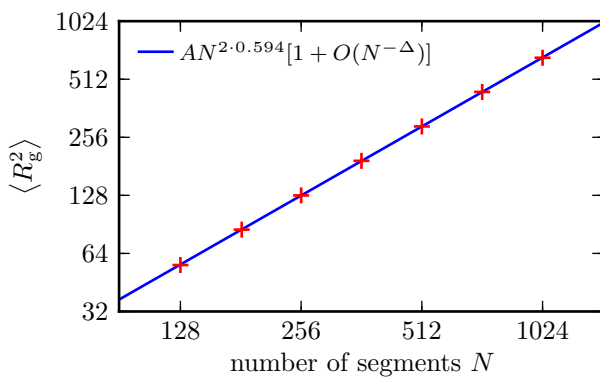
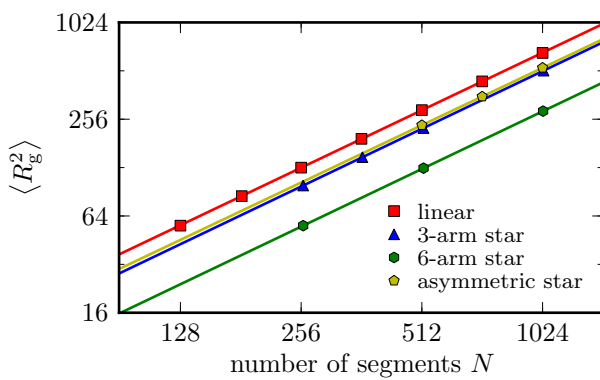
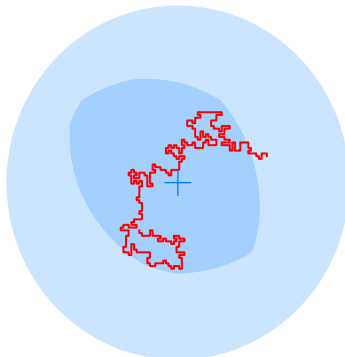
Figure 3.2: Scaling of linear chain.**Figure 3.3:** Scaling of 4 different architectures.

Figure 3.4: Accessible pore volume for a polymer chain. Accessible pore volume for center of mass of polymer chain is labeled by darker blue region.



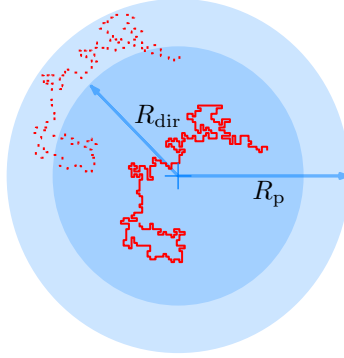
3.4 Distribution Coefficient Calculations

We mentioned already that we estimate various properties of branched polymers such as radius of gyration or hydrodynamic radius. Besides those one of the important task of polymer theorist is to predict elution behavior of branched polymers on size exclusion chromatography (SEC) also referred as gel permeation chromatography (GPC). As we mentioned in the introduction the SEC is one of the most prevalent characterization technique for synthetic and natural polymers. However despite a wide usage of SEC an ambiguity about its separation principle remains unresolved. It is generally believed that SEC is governed by equilibrium thermodynamics rather than hydrodynamics because the flow rates in experiments are generally quite low. On the other hand, work of Grubisic, Rempp and Benoit show that polymer molecules separates according their hydrodynamic volume regardless of their chemical composition and chain architecture. [22] And the hydrodynamic volume is of course dynamic quantity which points that this phenomenon is rather controlled dynamical properties of polymers.

In 1970s Casassa and co-workers developed an equilibrium theory for SEC of branched and linear chains which that the separation process is governed by the equilibrium partition coefficient, K , of solute macromolecules between a bulk dilute solution phase located at the interstitial space and confined solution phase within the pores of the column packing material. [23,24]

In general, the partition coefficient depend on the molecular size relative to the pore size. Since there are various measures of polymer coil size, the fundamental problem in the theory has been the choice of a proper molecular size parameter which correlates with, K . It has been shown before

Figure 3.5: Determination of the distribution coefficient. The shift distance at which chain touches the pore walls defines a volume. The average volume with respect to all direction divided by total pore volume gives the distribution coefficient, K , of a particular conformation.



that R_h is more suitable than R_g which fails to provide universal calibration curve. [9,24,25] Recently another parameter was considered to fit even better to fit this calibration curve for different architectures which is called the span dimension it is basically average radius of convex envelope of polymer. [22] We will however not discuss it here and we refer reader elsewhere. Despite the analytical calculation as well as simulation have been performed to show that R_h well follows the calibration curve for different architectures we recalculate this for even more complex architectures such as dendrimer and asymmetric H-shape ([50][100][200][300][400])). All calculated architectures are summarized in Table 3.2. Details on performed calculations follows.

The distribution coefficient is determined as a fraction of the pore volume accessible for a particular architecture (see Figure 3.4) [9]. For simulation of the distribution coefficient of a particular conformation we place a center of mass of the conformation in the center of pore with radius R_p , then we select a random direction and calculate a displacement vector R_{dir} at which conformation intersects with a wall (see Figure 3.5). Average over D directions gives an average displacement vector which denotes a sphere radius of volume of accessible fraction. Distribution coefficient is then evaluated as

$$K_{conf} = \frac{V_{acc}}{V_{pore}} = \frac{\left(\frac{1}{D} \sum_D R_{dir} \right)^3}{R_p^3}. \quad (3.18)$$

Figure 3.6: Graph of normalized root of average square of gyration radius, $\langle R_g^2 \rangle^{1/2}$, vs distribution coefficient K for different architectures, where R_p denotes the pore radius. It shows that calibration curve constructed using gyration radius differs for different architectures.

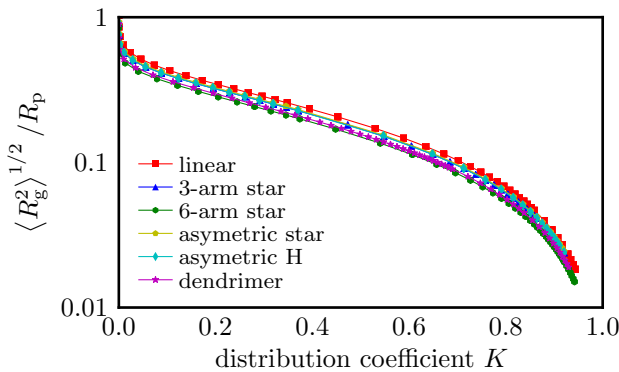


Figure 3.7: Graph of normalized average hydrodynamic radius, $\langle R_h \rangle$, vs distribution coefficient K for different architectures, where R_p denotes the pore radius. It shows that calibration curve constructed using hydrodynamic radius is suitable for evaluation the elation behavior of randomly branched polymers.

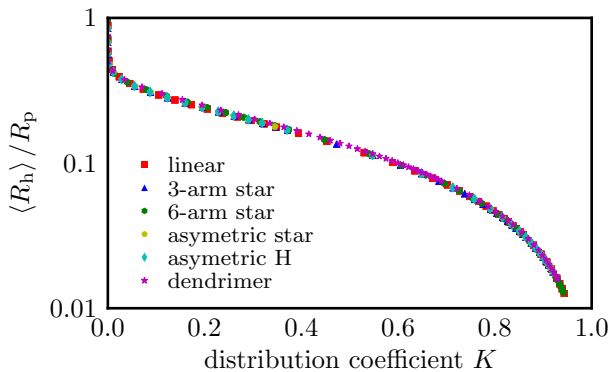


Table 3.2: Calculated architectures. On the table from left are snapshots of different architectures, schemes indicating lengths of particulars branches and their significant quantities, where N is total number of segments.

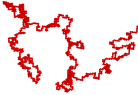
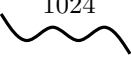
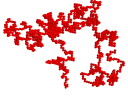
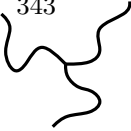

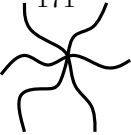
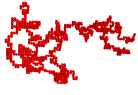
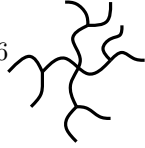
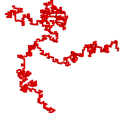
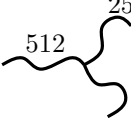
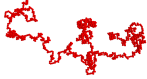
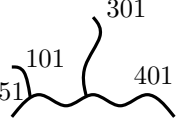
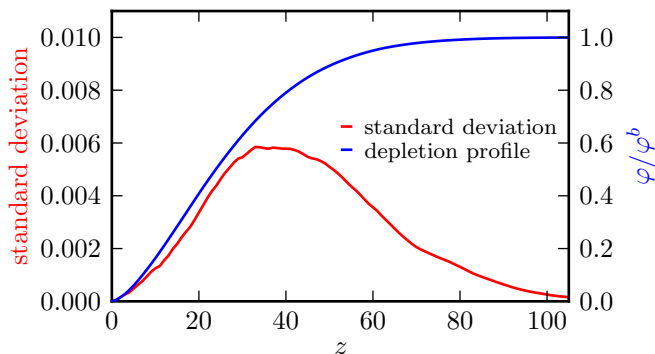
Architecture		N	$\langle R_g^2 \rangle^{1/2}$	R_h
	1024 	1024	25.72	17.68
	343 	1030	22.65	16.90
	171 	1027	16.95	14.47
	86 	1033	18.04	15.04
	254 512 	1024	23.12	16.93
	301 101 51 401 	1056	22.73	16.99

Figure 3.8: Depletion layer. We show depletion layer with error function depending on number of segments N .



The self-avoiding walks were generated on cubic lattice using dynamic Monte Carlo to simulate polymers in good solvent. We calculated normalized calibration curves for 6 different architectures: linear, 3-arm star, 6-arm star, dendrimer, 3-arm asymmetric star and asymmetric H-shape (see Table 3.2). All quantities were calculated within error of 1%. 32 trial direction were calculated to evaluate the distribution coefficient K . For calculation calibration curves we varied the radius of pore, R_p , instead of the chain size. Calculated calibration curves are shown in Figures 3.6 and 3.7. They show that hydrodynamic radius is suitable for predicting elution behavior of randomly branched polymers.

3.5 Depletion Layer Calculation

Depletion layer and depletion layer thickness are also important in the theory of SEC. We, however discuss it in more details in Chapter 4. Here, we only give simulation details on performed calculation of depletion layer. We calculate a depletion layer using generated MC conformations in the bulk, not in a vicinity of a wall. To calculate the depletion layer we put the conformation at certain distance from the wall and then we approach the conformation in one direction towards the wall. At each step we add up the histogram. When the conformation reaches the wall we stop. It is equivalent to generating MC at given distances from the wall but considering that if the SAW hits the wall we reject it. Conformations generated in such a way have than the same free energy. In principle you could generate the depletion layer in a same way as it is done for self-consistent-field calculation (Section 4.1)

this approach would be, however, computationally much more demanding since you would have to calculate profiles in many different distances from the wall and than you would also have to estimate the free energies of these profiles which can not be done very easily for MC calculations. In Figure 3.8 we show depletion layer of linear chain with $N=1024$ segments. And we show the standard deviation of the depletion layer calculated using the way described above. All the errors are within 1% we thus believe it is a relevant way to calculate depletion profiles from MC conformations.

3.6 Graph Theory Calibration

We are able to calculate quantities of randomly branched polymers such as radius of gyration or hydrodynamic radius using MC calculation. This is however quite time demanding. In some cases the computation time is crucial and we need to estimate these quantities in a very short time although they would be approximate. There is a method for finding the radius of gyration of the architectures of branched polymers using a statistical mechanical theory employing a graph-theoretical representation of the connectivity in the molecules. [26–28]

3.6.1 Graph Theory

Let us briefly outline how radius of gyration can be calculated from graph theory. The distribution function for the square radius of gyration R_g^2 of a system of N beads, which we here consider as a model for molecule with N monomer units, has been derived as [26]

$$P(R_g^2) dR_g^2 = \frac{dR_g^2}{2\pi} \int_{-\infty}^{\infty} e^{i\beta R_g^2} B(\beta) d\beta \quad (3.19)$$

where $B(\beta)$ is a characteristic function, here presented in a slightly modified form

$$B(\beta) = |\mathbf{I} + \frac{i\beta}{N} \Lambda_{N-1}^{-1}|^{-3/2}, \quad (3.20)$$

\mathbf{I} in the $(N-1) \times (N-1)$ identity matrix and Λ_{N-1}^{-1} is the matrix with $N-1$ reciprocals of eigenvalues of the Kirchhoff matrix \mathbf{K} , a graph-theoretical representation describing the connectivity between the N units. Kirchhoff matrix of a graph G where $G = G(V, E)$ is an undirected, unweighted graph, V is set of vertex, $V \equiv \{v_1, \dots, v_N\}$, $N = |V|$ and E is an edge set, is a $N \times N$ symmetric matrix, $\mathbf{K} := (k_{ij})_{N \times N}$, defined as

$$k_{ij}(G) = \begin{cases} \deg(v_i) & i = j \\ -1 & \text{if } i \neq j \text{ and } v_i \text{ is adjacent to } v_j \\ 0 & \text{otherwise.} \end{cases} \quad (3.21)$$

For example Kirchiv matrix of a star like architecture ($[2[1][3]]$) is written as

$$\mathbf{K} = \begin{pmatrix} 1 & -1 & 0 & 0 & 0 & 0 & 0 \\ -1 & 2 & -1 & 0 & 0 & 0 & 0 \\ 0 & -1 & 3 & -1 & -1 & 0 & 0 \\ 0 & 0 & -1 & 1 & 0 & 0 & 0 \\ 0 & 0 & -1 & 0 & 2 & -1 & 0 \\ 0 & 0 & 0 & 0 & -1 & 2 & -1 \\ 0 & 0 & 0 & 0 & 0 & -1 & 1 \end{pmatrix}. \quad (3.22)$$

The average square radius of gyration $\langle R_g \rangle$ follows from the first moment of this distribution eqn. (3.19) as [26]

$$\langle R_g^2 \rangle \langle l^2 \rangle = N^{-1} \text{Tr}(\Lambda_{N-1}^{-1}) \quad (3.23)$$

and is expressed in terms of the mean of the square length of the edges between units l^2 . The Kirchhoff matrix is derived from incidence matrix \mathbf{C} .

$$\mathbf{K} = \mathbf{C} \gamma \mathbf{C}^T \quad (3.24)$$

where \mathbf{C}^T is transpose of \mathbf{C} and $\gamma = 3/(2l_{ij}^2)$, l_{ij} is a length measure of the edge between beads i and j . Hence, γ is a vector of length $N - 1$. For all edges having equal length equation (3.24) becomes $\mathbf{K} = \gamma \mathbf{C} \mathbf{C}^T$ and equation (3.20) becomes

$$B(\beta) = |\mathbf{I} + \frac{-i\beta}{\gamma N} \Lambda_{N-1}^{-1}|^{-3/2}. \quad (3.25)$$

3.6.2 Coarse Graining

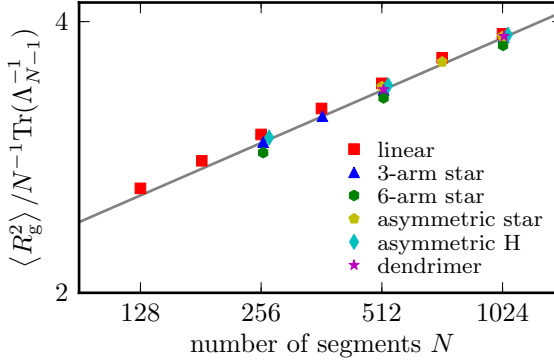
According to (3.23) for calculating radius of gyration of a molecule with N segments $N \times N$ Kirchhoff matrix has to be solved. However that means that for a molecule with a million segments a matrix of $10^6 \times 10^6$ we would have to find its smallest values. This is computationally very demanding if not practically impossible. Fortunately, this model can be coarse-grained in a very simple way within a reasonable error. [27] Assuming that length of a coarse grained edge $i - j$, originally consisting of N_{ij} unit segments, to equal the average end-to-end distance $\langle \mathbf{r}_{ij} \rangle$ of a linear chain consisting of N_{ij} segments. The $\langle \mathbf{r}_{ij} \rangle$ scales with root of the number of segments N_{ij} , so we accordingly assume l_{ij} to equal $N_{ij}^{1/2}$. γ thus becomes a vector the reciprocal value of the number of monomer units in each edge N_{ij}

$$\gamma = \frac{3}{2N_{ij}}. \quad (3.26)$$

Equation 3.23 can be then reformulated for evaluation R_g from a reduced matrix as

$$\langle R_g^2 \rangle \langle l^2 \rangle = \frac{N}{N_{\text{red}}^2} \text{Tr}(\Lambda_{N_{\text{red}}-1}^{-1}) \quad (3.27)$$

Figure 3.9: Logarithmic plot of mean square radius of gyration obtained from MC calculation $\langle R_g^2 \rangle$ divided by results from the graph theory for the same molecules vs. number of segments N .



where N_{red} is number of segments of reduced matrix, meaning that this new reduced matrix has segments length N/N_{red} . The error of this coarse-graining comes from neglecting contribution of very small eigen values. For more details we refer reader to [26,27].

3.6.3 Comparison of MC and Graph Theory

We compared results for a mean square radius of gyration for different architectures from MC calculations and from the graph theory. In Figure 3.9 we show logarithmic plot of mean square radius of gyration obtained from MC calculation $\langle R_g^2 \rangle$ divided by results from the graph theory, $N^{-1}\text{Tr}(\Lambda_{N-1}^{-1})$, for the same molecules vs. number of segments N . It displays that MC results could be estimated using

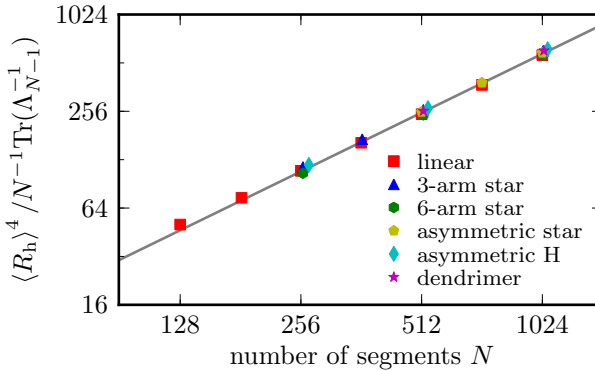
$$\frac{\langle R_g^2 \rangle}{N^{-1}\text{Tr}(\Lambda_{N-1}^{-1})} \approx A' N^{\nu'} \quad (3.28)$$

as

$$\langle R_g^2 \rangle \approx A' \text{Tr}(\Lambda_{N-1}^{-1}) N^{\nu'+1}. \quad (3.29)$$

Enqs. (3.28) and (3.29) are in accord with graph-theory representation because it uses Gaussian chain model to derive eqn. (3.19). Meaning that graph-theory represents an ideal chain which, of course, follows different scaling. If they had the same scaling the scaling exponent should be close to one. We see that preexponential factor in eqn. (3.29) differs for different architecture but there is still a good quantitative agreement of MC and

Figure 3.10: Logarithmic plot of mean hydrodynamic radius to power of 4 obtained from MC calculation $\langle R_g \rangle$ divided by results from the graph theory for the same molecules vs. number of segments N .



graph-theory representation results. The preexponential factor A' and the scaling exponent ν' can be obtained by numerical fitting. We estimated them to be $A' = 1.00 \pm 0.05$ and $\nu' = 0.194 \pm 0.005$, however different fit can be used as well (e.g. the data can be fitted using only the linear chain). The eqn. (3.29) can be then used for, although approximate, a very fast estimation of mean square radius of gyration, $\langle R_g \rangle$, for different architectures.

3.6.4 Hydrodynamic Radius Calibration

As we discussed in Section 3.4 for predicting elution behavior of branched macromolecules we are rather interested in hydrodynamic radius than in evaluation of radius gyration. Although eqn. (3.23) is not meant to give a value of hydrodynamic radius R_h it can still be used as a measure of "branchiness" of polymer, i.e. how much is a polymer branched regarding position of branch points and length of links. According to Figure 3.9 such measure seems reasonable. Since the hydrodynamic radius also follows scaling behavior although the scaling exponent is different from the scaling exponent of radius of gyration or end-to-end distance Proceeding the same way as above, i.e. comparing radius of gyration, we can receive a similar graph to Figure 3.9 but the preexponential factors of different architectures differs significantly. However, we show that it is possible to introduce a calibration to fit MC data with graph-theory which leads to

$$\langle R_h \rangle^4 \approx A^* \text{Tr}(\Lambda_{N-1}^{-1}) N^{\nu^*+1}. \quad (3.30)$$

This dependence is plotted in Figure 3.10. Calibration gives preexponential factor $A^* = 0.128 \pm 0.015$ and $\nu^* = 1.216 \pm 0.018$. Using the calibration you can estimate the MC result for hydrodynamic radius within an error of 3% (for $N \in (128, 1056)$) in a very short time corresponding to the time needed for solving the eigenvalue problem of a Kirchhoff matrix. We stress that this agreement is achieved by numerical fitting and we have no theoretical evidence for that. For further discussion a proper derivation of the hydrodynamic radius from graph theory is needed. We suggest that this calibration can be with advantage used to predict elution behavior of randomly branched architectures obtained from stochastic kinetics simulations. [27–30]

CHAPTER 4

Self-Consistent Field Method for Polymers

We have performed Monte Carlo (MC) simulations and self consistent (SCF) field calculations to analyze the depletion profiles for linear, star-like and H-shaped polymers in good solvent using lattice approximations in both methods. In the SCF approach the intra-molecular excluded volume-effects are accounted for using an approach that resembles Flory's argument that leads to the Flory size of the chains. This gives a major improvement over the classical tanh profile, and becomes much closer to the MC results, provided that a Kuhn length of 1.5 is implemented.

4.1 Introduction

Polymers that are near non-adsorbing surfaces display the depletion phenomenon. Compared to the possible conformations in the bulk solution, as soon as the center of mass of the macromolecules is closer to the boundary than the natural size, $h < R_g$, the number of allowed conformations are reduced. As a consequence a depletion layer develops with thickness δ which again is of the order of the coil size. [23, 24]

Size exclusion chromatography makes use of this depletion profile to separate macromolecules with different values of R_g . [31, 32] Polymer depletion is also important for the colloidal stability, albeit that the interactions become relevant when the polymer concentration is near the overlap concentration. [33]

To model the depletion zone near a non-adsorbing surface, one can use the Edwards equation. The classical result, applicable for Gaussian chains, is known for a long time. This result is reasonable for chains in a theta solvent $\chi = 0.5$. However, in good solvent this result is known to be very approximate. The simple reason is that the coil sizes in good solvent are

larger than the Gaussian dimensions because of excluded volume effects. It is complicated to introduce intra-molecular excluded-volume effects rigorously. Below we will introduce a new route which makes use of the self-consistent field Ansatz to evaluate the depletion profile for chains that swell due to their excluded volume. The key idea is to consider conformations of chains with a constraint on the central segment of the chain is located at a specified coordinate. In this way the chain will feel its excluded volume in a Flory-like fashion. Of course the results are not exact, because in a real chain, each segment along the chain has its own excluded volume effects and the central segment has no special property. Nevertheless we argue that this Flory-like approach is of use to predict the depletion of architecturally complex molecules (as well as linear chains).

An alternative way to evaluate the depletion profile is to use the Monte Carlo (MC) approach. With MC it is possible to generate self-avoiding chain conformations and evaluate the radius of gyration from this. In dilute solutions, one can use the same conformations to predict the depletion profile.

In this part of our work we compare predictions of the SCF method sketched above with MC simulations using similar models, namely for flexible polymers on a cubic lattice in good solvent. We compare result for linear chains, stars and H-like chains.

First we will give some preliminary considerations of the depletion problem. This is followed by some details of the SCF method. [34] The details of the MC calculation are presented in Section 3.5. Before discussing our results we will go into some details how the models that have been used are matched. In the end we formulate our conclusions and speculate how the SCF method may still be improved to obtain an even better match with MC.

4.2 SCF Theory

Here we give reader some background of the SCF theory. More on the SCF theory can be found in the textbook [34]. We consider the standard depletion conditions. More specifically we consider isolated polymer chains in a good monomeric solvent in contact with a flat non-adsorbing surface. The classical theory starts with the Edwards equation

$$\frac{\partial G(\mathbf{r}; s)}{\partial s} = \frac{1}{6} \nabla^2 G(\mathbf{r}; s) - u(\mathbf{r}) G(\mathbf{r}; s) \quad (4.1)$$

where u is segment potential and G is the end-point distribution function. Below we will discretized space by using a lattice and solve this equation using the Scheutjens Fler machinery (SF SCF). In this approach there exists at each coordinate \mathbf{r} a value for the segment volume fraction given

by φ_p (dimensionless segment concentration) and a solvent volume fraction φ_s that locally obey the incompressibility constraint $\varphi_p + \varphi_s = 1$. In the good solvent it can be shown that the dimensionless potentials that obey this constraint are given by

$$u(\mathbf{r}) = -\frac{\ln \varphi_s(\mathbf{r})}{\ln \varphi_s^b}. \quad (4.2)$$

In dilute solutions and for non-adsorbing chains there is just one relevant coordinate $\mathbf{r} = z$ (i.e. distance from the wall) and the potential as given by 4.2 reduces to $u(z) \approx 0$. Taking the boundary condition $G(0, s) = 0$, it is possible to find an exact solution [35] for the end point distribution

$$\varphi_e(z) = \operatorname{erf} \frac{z}{2R_g}, \quad (4.3)$$

with $R_g = b\sqrt{N/6}$ is the radius of gyration with b the segment size and N the number of segments in the (linear) chain. To a very good approximation [36] it is shown that the depletion profile obeys

$$\varphi_p(z) = \varphi_p^b \tanh z/\delta_0 \quad (4.4)$$

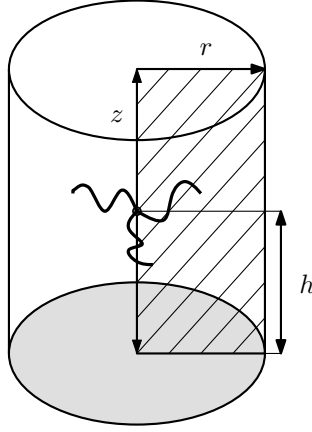
where the depletion layer thickness, δ_0 , is closely related to the gyration radius

$$\delta_0 = \frac{2}{\sqrt{\pi}} R_g. \quad (4.5)$$

It must be understood that the exact result for the Edwards equation in the case of depletion from dilute solutions is a mean field result. It applies for Gaussian chains that have no intra-molecular excluded-volume effects. The SF SCF method that is elaborated below, maps the Edwards equation onto a lattice and by doing so, the chain model becomes a freely-jointed chain, rather than the Gaussian chain. The difference in chain models is minor. Hence, the SF SCF result for depletion layer is nearly identical to that for Gaussian chains. The issue is that the classical SF SCF method also ignores the intra- and inter-molecular excluded-volume effects, especially for dilute solutions.

Using Flory arguments (Section 1.3.4) we estimated $R_g^F \propto N^{3/5}$. A more reasonable result for the depletion layer thickness would therefore be $\varphi_p(z) = \varphi_p^b \tanh z/\delta$ with $\delta \approx R_g^F$. In words, the depletion layer thickness should, in good solvent, be given by the size of the swollen coil, rather than that of the unperturbed one.

Below we will elaborate on an extended SF SCF procedure for depletion from dilute solutions, which significantly improves over the classical method by accounting (in an approximate way) for the intra-molecular excluded volume effects. The key idea is to consider all possible conformations of a

Figure 4.1: Cylindrical coordinates

polymer chain which has a central segment along its architecture fixed to a specified location. Linear chains are thus represented as a two-armed star, which the center fixed to a location on the lattice. The solution of the SCF equations for such a star gives a coil size that is consistent with R_g^F . [37, 38] This idea is implemented in a two-gradient cylindrical coordinate system. In this coordinate system it is possible to combine a flat surface with a chain fixed at a specified coordinate above this surface.

4.2.1 Self-Consistent Field Theory and the Molecular Model

From the above it is clear that we need to develop the SF SCF formalism for the case that there is an f -armed star, (the $f = 2$ star corresponds to linear chains), with each arm of length N_{arm} , so that the overall number of segments is given by $N = fN_{\text{arm}} + 1$ (the unity is added to account for the segment X in the center). We use a two-gradient cylindrical coordinate system $\mathbf{r} = (z, r)$ (Figure 4.1), where layers $z = 1, \dots, z_M$ are parallel to a flat impenetrable (inert) surface (positioned at $z = 0$). The size of a lattice site is set equal to the size of a segment given by b . Below all linear lengths are made dimensionless by this length and therefore b is typically omitted from the equations. In each layer there are concentric rings of lattice sites $r = 1, \dots, r_M$, such that the number of lattice sites at $L(z, r) = \pi(r^2 - (r-1)^2) = \pi(2r-1)$. We will apply the mean field approximation over all sites for given (z, r) . The star is, with its central segment, positioned at a height h above the surface, or more precisely, the pinning site is at $(z_p, r_p) = (h, 1)$. The goal is to evaluate both the free energy of the star at a height h , $F(h)$, as well as the volume fraction distribution $\varphi_p^{(h)}(\mathbf{r})$. From

this the depletion profile follows as

$$\frac{\varphi(z)}{\varphi^b} = \frac{1}{N} \sum_h \sum_r L(z, r) \varphi_p^{(h)}(z, r) \exp -\Delta F(h) \quad (4.6)$$

where $\Delta F(h) = F(h) - F(\infty)$ in units of the thermal energy $k_B T$. It is easily checked that, for large values of z , this normalized profile goes to unity.

Both the $\varphi_p^{(h)}(z, r)$ as well as the corresponding free energy $F(h)$ are readily available from the SF SCF calculations. The approach starts with a free energy (in units of $k_B T$) that, in our case, is written as

$$F(h) = -\ln Q^{(h)} - \sum_{\mathbf{r}} u(\mathbf{r}) L(z, r). \quad (4.7)$$

Where the segment potentials (cf eqn. 4.2) will, of course, also depend on the location where the star is pinned. The single chain partition function $Q[u]$ is computed from the segment potentials. In general one has to account for the statistical weight of all possible conformations of the chain(s) in the system. In our case there is just one chain, pinned with the central segment to location $(h, 1)$. We use the Edwards equation to obtain this partition function. The chain model that results from mapping the Edwards equation to the discrete lattice leads to a freely jointed chain (FJC) model.

In the FJC model there exists an efficient way to compute the volume fraction distribution and to obtain the partition function, which is referred to as the propagator scheme. Let us first introduce the Boltzmann weights that contains the segment potential

$$G(\mathbf{r}) = \exp [-\mathbf{u}(\mathbf{r})] \quad (4.8)$$

which may be interpreted as the probability to find a segment at location \mathbf{r} if it was not connected to the chain. We consider, for simplicity, a chain with a symmetric topology of the f -armed star: $(A)_{N_{\text{arm}}} (X)_1 [(A)_{N_{\text{arm}}}]_{f-1}$. For the cases that the chains have a more complex topology we refer to the literature. [39] The procedure features a pair of complementary propagators, a forward and a backward one.

Going towards the center of the star, we compute the forward end-point distribution function $G(\mathbf{r}; s|1)$. As compared to eqn. (4.1) we have extended the notation for the end-point distribution functions. The unity behind the vertical bar indicates that we have started with the free end

$$G(\mathbf{r}; s+1|1) = G(\mathbf{r}) \sum_{\mathbf{r}'} \lambda(\mathbf{r}|\mathbf{r}') G(\mathbf{r}'; s|1). \quad (4.9)$$

This equation is started with putting $G(\mathbf{r}; 0|1) = 1$ for all coordinates \mathbf{r} with $z > 0$ (unrestricted start) and $G(0, r; 0|1) = 0$ (chains can not be

initiated in the plane of the surface). In eqn. (4.9) we have the *a priori* step probabilities to go from $\mathbf{r}' \rightarrow \mathbf{r}$. In a FJC on a cubic lattice there are six neighboring sites. This leads to λ 's with the following weights

$$\lambda(z, r|z-1, r) = \frac{1}{6} \quad (4.10)$$

$$\lambda(z, r|z+1, r) = \frac{1}{6} \quad (4.11)$$

$$\lambda(z, r|z, r-1) = \frac{1}{6} \frac{2r}{2r-1} \quad (4.12)$$

$$\lambda(z, r|z, r+1) = \frac{1}{6} \frac{2r+2}{2r-1} \quad (4.13)$$

$$\lambda(z, r|z, r) = \frac{2}{6} \quad (4.14)$$

where eqns. (4.12) and (4.13) have r dependencies to account for the fact that the number of available sites $L(z, r)$ is growing linearly with r . The propagator terminates at the central segment $s = N_{\text{arm}} + 1$.

Next, we have to propagate from the center of the star back to the free end of the star. This leads to backward end-point distribution functions $G(\mathbf{r}; s|h, 1; N_{\text{arm}} + 1)$ where the variables behind the vertical bar indicate that segment $s = N_{\text{arm}} + 1$ is at $(h, 1)$

$$G(\mathbf{r}; s|h, 1; N_{\text{arm}} + 1) = G(\mathbf{r}) \sum_{\mathbf{r}'} \lambda(\mathbf{r}|\mathbf{r}') G(\mathbf{r}'; s+1|h, 1; N_{\text{a}} + 1). \quad (4.15)$$

Again, the start of the propagator is constrained: segment $s = N_{\text{arm}} + 1$ must be located at $(h, 1)$ and accounting for all $f - 1$ remaining arms we may use

$$G(h, 1; N_{\text{arm}} + 1|h, 1; N_{\text{arm}} + 1) = G(h, 1; N_{\text{arm}} + 1|1)^{f-1} / G(h, 1)^{f-2} \quad (4.16)$$

and zero for all $\mathbf{r} \neq (h, 1)$. The normalization by $G(h, 1)^{f-2}$ is necessary because the statistical weight for the central segment must be given only once.

The propagators terminate when the chain is at the free end. From the resulting end-point distribution we can evaluate the single chain partition function

$$Q = \sum_z \sum_r L(z, r) G(z, r; 1|h, 1; N_{\text{arm}} + 1). \quad (4.17)$$

The volume fraction distribution for the full f -armed star can be computed using the composition law:

$$\varphi^{(h)}(\mathbf{r}) = \sum_{s=1}^{N_{\text{arm}}} \frac{f}{Q} \frac{G(\mathbf{r}; s|1) G(\mathbf{r}; s|h, 1; N_{\text{arm}} + 1)}{G(\mathbf{r})}. \quad (4.18)$$

The division by $G(\mathbf{r})$ is necessary to correct for the point that each segment received the weight both from the forward and the backward propagator. The multiplication with f reflects the point that each arm has the same contribution to the volume fractions. The division by the partition function guarantees that there is exactly one full star in the system. The central segment X has a contribution $\varphi(h, 1) = 1/L(1)$ to the overall volume fraction distribution which must be added to the result of eqn 4.18.

The volume fraction of the solvent monomers simply follows from the Boltzmann equation

$$\varphi_s(\mathbf{r}) = \varphi_s^b G(\mathbf{r}) = G(\mathbf{r}) \quad (4.19)$$

where it is implemented that in the present system the volume fraction of solvent in the bulk is unity.

Summarizing, it is shown that the segment potentials depend on the volume fractions (cf Eqn 4.2), and that the volume fractions $\varphi^{(h)}(\mathbf{r})$ and $\varphi_s(\mathbf{r})$ are a function of the potentials (cf Eqns 4.8 to Eqn 4.6 and Eqn 4.19). Only when the potentials and volume fractions are consistent with each other, we have optimized the free energy and can evaluate eqn 4.7. Such self-consistent field point is found numerically. Routinely we obtain results that have at least 7 significant digits. Details are given elsewhere. [40]

4.3 The Models

One of the obvious approximations that is inherent to the freely jointed chain is the fact that short-range excluded volume correlations along the chain are only partially implemented. The 6-choice propagator, which is discussed above, ensures that two neighboring segments s and $s + 1$ along the chain occupy neighboring lattice sites. However, $s - 1$ and $s + 1$ may be on the same lattice site. This is characteristic for a first order Markov chain. In principle one can correct for this by implementing by implementing an extended propagator, implementing a longer history. [41] For example one can implement a second order Markov chain approximation where direct backfolding is prohibited. This leads to a so-called 5-choice propagator. When only backfolding is blocked and the chain remains further fully flexible, it is known that the Kuhn length becomes 1.5 segments. In first order one thus replace a chain in the 5-choice propagator with N segments by a chain in the 6-choice lattice using a renormalized number of segments $N^{(5\text{-choice})} = N^{(6\text{-choice})}/1.5$ segments, each with a length $b^{(5\text{-choice})} = b^{(6\text{-choice})}1.5$ length.

One of the targets of this work is to compare MC results, where chains are fully self-avoiding, with corresponding results from SF SCF calculations. It is clear that the models for both approaches should match. Here we insist on the idea that results for the SF SCF model with the renormalized number of segments and renormalized segment length should be compared with MC

results for the unnormalized values for the number of segments with the unnormalized lengths. When result of the two approaches are compared we have implemented that the length scale in the SCF is transformed into those used in MC (that means that all linear lengths in SCF are multiplied by 1.5).

Results are generated in both approaches for a series of chain architectures ranging from linear chains ($f = 1$, and $f = 2$) to stars up to $f = 6$. There are also results for stars with lengths of arms that are not all the same and for architecturally more complex molecules having an H-shape. The latter molecules are treated using some more complicated propagator formalism for which we refer to the literature. [39]

CHAPTER 5

Comparison of MC and SCF Results

We present data from comparison of MC and SCF depletion layer calculations in Table 5.1. We show the root of mean square radius of gyration $\langle R_g \rangle^{1/2}$ and the depletion layer thickness δ for calculated architectures, i.e. linear ($N = 1024$), 3-arm star ($N = 1030$), 6-arm star ($N = 1027$) and H-shape ($N = 1006$). You can see that MC results for radius of gyration compare quite well with SCF results where 1.0 Kuhn length is implemented. On the other hand, the results for the depletion layer thickness, δ_0 , compare better with SCF where 1.5 Kuhn length implemented.

In all figures the GSA denotes the ground state approximation, i.e. SCF results without a pinned segment. In Figures 5.1 and 5.2 we show comparison of depletion layers obtained from MC and SCF calculation. There, you can see from the graph, what we already mentioned, that SCF with 1.5 Kuhn length gives a better agreement than using the SCF with 1.0 Kuhn length implemented. For this reason in the rest of graphs we show only a comparison of MC and SCF 1.5, i.e. with 1.5 Kuhn length implemented. In Figures 5.3 and 5.4 we show depletion layers of 3-arm star and 4-arm star. From these graphs you can see that depletion layer becomes more accurate as the number of arms increases. The last is the Figure 5.5. There we show H-shape polymer with pin-point once in the center (H-shape_c) and then in the branching point (H-shape_b). It shows that it is more reasonable to pin the branching point rather than the center of the H-shape polymer. Further discussion follows.

5.1 Discussion

SCF results and MC results are in good quantitative agreement, both for the coil size as well as the depletion layer thickness. Also there is a

Table 5.1: MC and SCF data

	$\langle R_g \rangle^{1/2}$			δ_0			
	MC	SCF	SCF 1.5	MC	SCF	SCF 1.5	
linear	25.72	33.60	40.12	27.48	24.32	28.86	(1)
		25.11	29.98		24.19	28.80	(2)
3-arm star	22.66	21.29	25.44	26.46	23.05	27.55	
6-arm star	16.95	15.99	19.12	22.89	20.09	24.05	
H-shape	21.51	22.63	26.99	25.42	22.28	26.60	(b)
		21.76	25.94		22.82	27.21	(c)

(1) stands for 1-arm star, (2) stands for 2-arm star, (b) is a H-shape polymer pinned at the branching point and (c) is a H-shape polymer pinned at the center. SCF 1.5 signifies that 1.5 Kuhn length was implemented.

Figure 5.1: 1-arm star

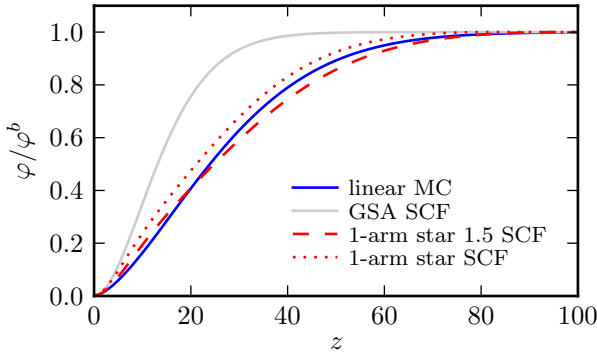


Figure 5.2: 2-arm star

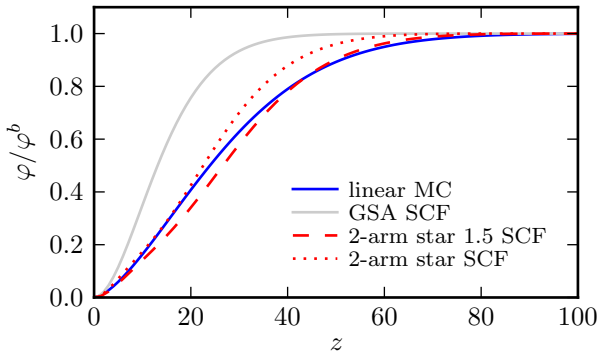
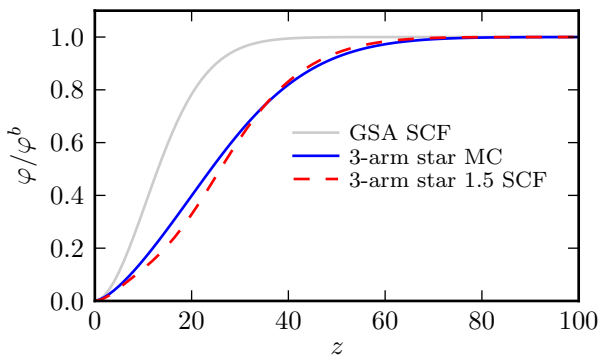
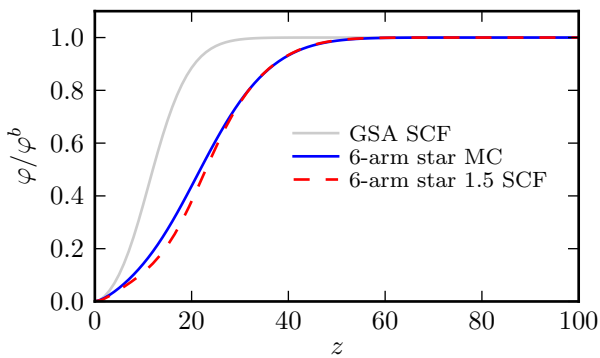
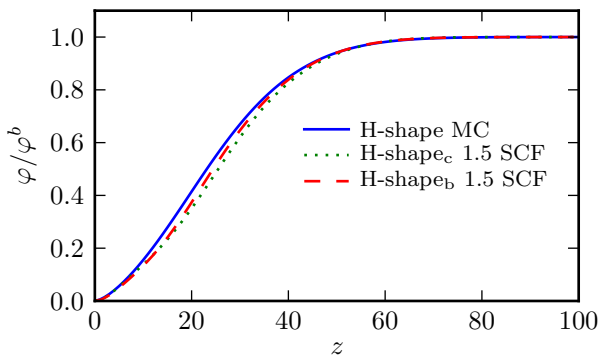


Figure 5.3: 3-arm star**Figure 5.4: 6-arm star****Figure 5.5: H-shape polymer**

reasonable agreement on the depletion profile. Small systematic differences were detected which point to the approximate nature of accounting for intra-molecular excluded volume in the SCF method. Possible suggestion to improve on this are discussed below.

For fixed overall molecular weight, increasing the number of arms, implies a more compact structure. The R_g is decreasing with the number of arms and the corresponding depletion thickness also decreases. This trend is present in both approaches and the SCF results follow the MC results almost quantitatively. Indeed, it is found that the results of SCF improve with the increase in the number of arms. A multi-arm star is, by its construction isotropic and therefore the mean field approximation is gradually more accurate. According to that, however, we expect that the SCF result for the linear star is more approximate because of the pre-assumption that the coils are rotationally symmetric breaks down for low values of f .

We have considered the depletion layer in dilute solutions. In this limit the thickness of the depletion layer is given by the radius of gyration R_g . At higher concentrations, and in particular in semi-dilute solutions, the thickness of the depletion layer depends on the concentration. Recently, Charlaganov and coworkers [42] showed that a combination of a MC approach and SCF allows to model semi-dilute solutions in such a way that the inter and intra-molecular excluded volume effects are (again on the Flory level) accounted for. As a result it was shown that the depletion layer thickness scaled proportional to the bulk correlation length and the de Gennes scaling exponent $\alpha = -4/3$ was recovered.

The idea implemented by Charlaganov *et al.* is rather simple. They treated in a 3d volume a set of molecules for which the centers of mass were generated using the MC scheme and the conformational degrees of freedom using the discrete version of the Edward equation (similarly as it is the presented here). It was already discussed that possible improvements of the excluded volume problem may involve the modeling of chains with multiple pinned segments, whereas the remainder degree of conformational degrees of freedom are evaluated using the Edwards equation.

The detailed comparison of SF SCF and MC results for the depletion profiles revealed systematic deviations. The depletion profile in MC takes a longer distance to approach the bulk value and has close to the surface a higher polymer density. Hence, the depletion profile is less steep in MC than in SF SCF. These deviations also point to the approximate nature of how the intra-molecular excluded volume is accounted for in the current SF SCF method. In the current approach there is just one segment which is pinned at some position in the coordinate system. This pinned segment generates a crowding of segments in its direct environment. This causes the chain to swell away from the pinned segment. The mean field approximation subsequently enforces a rotational symmetry of the resulting density

profile. More specifically, this prevents the formation of anisotropic coils. Yet, it is known that chain conformations, especially for linear chains, are not isotropic at all. Considering two points with excluded volume (for example the two ends of the chain), and optimizing the distance between these two points, may largely correct for this flaw. Implementing this idea for the depletion problem is expected to improve the match between SCF and MC.

Below we insisted on using in SCF the Kuhn length of 1.5. This introduced a difference in number of segments used in SCF and in MC. For the case of linear chains and stars with few arms, we believe that the current approach is reasonable. Of course it is possible to develop the second order Markov approach in SCF and then the models in SCF and MC match by construction better. Results for this approach will be discussed elsewhere.

References

- [1] M. RUBINSTEIN and R. H. COLBY, *Polymer Physics*, Oxford University Press Inc., New York, 2003.
- [2] A. Y. GROSBERG and A. R. KHOKHLOV, *Statistical Physics of Macromolecules*, AIP Press, New York, 1994.
- [3] M. DOI and S. F. EDWARDS, *The Theory of Polymer Dynamics*, Oxford University Press, New York, 1986.
- [4] P.-G. DE GENNES, *Scaling Concepts in Polymer Physics*, Cornell University Press, Ithaca, London, 1979.
- [5] J. C. LE GUILLOU and J. ZINN-JUSTIN, *Physical Review B* **21**, 3976 (1980).
- [6] G. PARISI, *Physics Reports* **49**, 215 (1979).
- [7] R. GUIDA and J. ZINN-JUSTIN, *Journal of Physics A: Mathematical and General* **31**, 8103 (1998).
- [8] M. MUTHUKUMAR and B. G. NICKEL, *The Journal of Chemical Physics* **86**, 460 (1987).
- [9] W. RADKE, *Macromolecular Theory and Simulation* **10**, 668 (2001).
- [10] M. H. KALOS and P. A. WHITLOCK, *Monte Carlo Methods*, Wiley-VCH Verlag GmbH Co., Weinheim, 2008.
- [11] D. FRENKEL and B. SMIT, *Understanding Molecular Simulation: From Algorithm to applications*, Academic Press, San Diego, 2002.
- [12] M. P. ALLEN and D. J. TILLESLEY, *Computer Simulation of Liquids*, Oxford University Press Inc., New York, 1997.
- [13] W. H. PRESS, S. A. TEUKOLSKY, W. T. VETTERLING, and B. P. FLANNERY, *Numerical Recipes in C: The Art of Scientific Computing, Second Edition*, Cambridge University Press, Cambridge, 1992.

- [14] N. METROPOLIS, A. W. ROSENBLUTH, M. N. ROSENBLUTH, and A. H. TELLER, *The Journal of Chemical Physics* **21**, 1088 (1953).
- [15] N. G. VAN KAMPEN, *Stochastic Processes in Physics and Chemistry*, Elsevier, Amsterdam, 1997.
- [16] M. N. ROSENBLUTH and A. W. ROSENBLUTH, *The Journal of Chemical Physics* **23**, 356 (1955).
- [17] K. BINDER, *Monte Carlo and Molecular Dynamics in Polymer Science*, Oxford University Press, New York, 1995.
- [18] D. E. KNUTH, *The Art of Computer Programming*, volume Fundamental Algorithms, Addison-Wesley Publishing Company, Reading, 1969.
- [19] H. FLYVBJERG and H. G. PETERSEN, *Journal of Chemical Physics* **91**, 461 (1989).
- [20] T. BIRSHTEN and E. ZHULINA, *Polymer* **25**, 1453 (1984).
- [21] B. LI, N. MADRAS, and A. D. SOKAL, *Journal of Statistical Physics* **80**, 661 (1995).
- [22] Y. WANG, I. TERAOKA, F. Y. HANSEN, G. H. PETERS, and O. HASAGER, *Macromolecules* **43**, 1651 (2010).
- [23] E. F. CASASSA, *Journal of Polymer Science Part B: Polymer Letters* **5**, 773–778 (1967).
- [24] E. F. CASASSA and Y. TAGAMI, *Macromolecules* **2**, 14 (1969).
- [25] W. RADKE, *Journal of Chromatography A* **1028**, 211 (2004).
- [26] B. E. EICHINGER, *Macromolecules* **13**, 1 (1980).
- [27] P. D. IEDEMA and H. C. J. HOEFSLOOT, *Macromolecular Theory and Simulation* **10**, 870 (2001).
- [28] P. D. IEDEMA and H. C. J. HOEFSLOOT, *Macromolecules* **69**, 3081 (2006).
- [29] D. T. GILLESPIE, *The Journal of Physical Chemistry* **81**, 2340 (1977).
- [30] J. HE, H. ZHANG, and Y. YANG, *Macromolecular Theory and Simulation* **4**, 811 (1995).
- [31] W. W. YAU, J. J. KIRKLAND, and D. D. BLY, *Modern Size Exclusion Liquid Chromatography*, John Wiley, New York, 1979.

- [32] H. PASCH and B. TRATHNIGG, *HPLC of Polymers*, Springer, Berlin, 1997.
- [33] G. J. FLEER and R. TUINIE, *Advances in Colloid and Interface Science* **143**, 1 (2008).
- [34] G. FLEER, M. C. STUART, J. SCHEUTJENS, T. COSGROVE, and B. VINCENT, *Polymers at Interfaces*, Chapman & Hall, London, 1993.
- [35] E. EISENRIEGLER, *Physical Review E* **55**, 3116 (1997).
- [36] R. TUINIER, G. A. Vliegenthart, , and H. N. W. LEKKERKERKER, *Journal of Chemical Physics* **113**, 10768 (2000).
- [37] J. VAN MALE, *Self-consistent-field theory for chain molecules: extensions, computational aspects, and applications*, PhD thesis, Wageningen University, the Netherlands, 2003.
- [38] B. R. POSTMUS, F. A. M. LEERMAKERS, and M. A. C. STUART, *Langmuir* **24**, 1930 (2008).
- [39] M. CHARLAGANOV, P. KOŠOVAN, and F. A. M. LEERMAKERS, *Soft Matter* **5**, 1448 (2009).
- [40] O. A. EVERS, J. M. H. M. SCHEUTJENS, and G. J. FLEER, *Macromolecules* **23**, 5221–5233 (1990).
- [41] C. C. VAN DER LINDEN, F. A. M. LEERMAKERS, and G. J. FLEER, *Macromolecules* **29**, 1172–1178 (1996).
- [42] M. CHARLAGANOV and F. A. M. LEERMAKERS, *Journal of Chemical Physics* **131**, 244115 (2009).